Journal of Computational and Applied Mathematics 491 (2027) 117987

Contents lists available at ScienceDirect

Journal of Computational and Applied Mathematics

journal homepage: www.elsevier.com/locate/cam

On L^2 approximation by spatial Pythagorean–hodograph curves

Rida T. Farouki [a], Marjeta Knez [b,c,*], Vito Vitrih [d,e], Emil Žagar [b,c]

[a] Mechanical & Aerospace Engineering, University of California, Davis, CA, 95616, USA
[b] Faculty of Mathematics and Physics, University of Ljubljana, Jadranska 19, Ljubljana, Slovenia
[c] Institute of Mathematics, Physics and Mechanics, Jadranska 19, Ljubljana, Slovenia
[d] Faculty of Mathematics, Natural Sciences and Information Technologies, University of Primorska, Glagoljaška 8, Koper, Slovenia
[e] Andrej Marušič Institute, University of Primorska, Muzejski trg 2, Koper, Slovenia

ARTICLE INFO

Keywords:
L^2 approximation
Quaternions
Pythagorean–hodograph curves
B splines
Preimage

ABSTRACT

Two methods for the L^2 approximation of smooth space curves by spatial Pythagorean–hodograph (PH) curves are considered. The first method employs direct approximation in $\mathbb{R}^3$, which results in a non–linear system of equations that may be solved by a numerical iteration or optimization scheme. The second method performs the optimization in the quaternion preimage space of PH curves, which results in a *linear* system of equations. The preimage of a curve in $\mathbb{R}^3$ is a *surface* in the quaternion space, and an appropriate locus on this surface must be identified for the given space curve. This is accomplished by observing that PH curves equipped with a rational rotation–minimizing frame (RMF) have preimages that are geodesic loci on the surface, and computing a discretized approximation to the RMF on the given curve. The methods are also extended to the approximation of spatial B–spline curves. Detailed algorithm descriptions are provided for both methods, and several computed examples illustrate their performance.

1. Introduction

Pythagorean–hodograph (PH) curves incorporate special algebraic structures that facilitate an exact computation of properties of interest in fields such as computer–aided geometric design, real–time motion control, computer animation, and related disciplines [1]. Thus, it is advantageous to develop methods that can closely approximate general parametric curves by PH curves.

The standard paradigm for constructing planar or spatial PH curves relies on a nonlinear mapping from a preimage space to Cartesian coordinates in order to obtain the curve derivative, known as the *hodograph*. In particular, the complex numbers $\mathbb{C}$ and the quaternions $\mathbb{H}$ serve as the appropriate preimage spaces for constructing the hodographs of PH curves in $\mathbb{R}^2$ and $\mathbb{R}^3$, respectively.

A classical approach to approximating parametric curves in a vector space equipped with a norm induced by an inner product is the L^2 approximation method, which projects a given curve onto a chosen finite dimensional subspace. However, when applied to approximation by PH curves, this method yields nonlinear equations whose solution methods may be computationally expensive or unreliable. To address these issues, an alternative approach has been proposed in [2] for approximations by planar PH curves, which involves an inverse–mapping of the curve to be approximated to the preimage space. The resulting problem then incurs only the solution of *linear* equations, and yields solutions close in accuracy to those of the non–linear approach.

The present study extends this approach to the case of spatial PH curves, in which the mapping of the hodograph of a given curve to the preimage space is more involved. Specifically, for any given spatial parametric curve, the preimage of its hodograph is not a

* Corresponding author.
E-mail addresses: farouki@ucdavis.edu (R.T. Farouki), marjetka.knez@fmf.uni-lj.si (M. Knez), vito.vitrih@upr.si (V. Vitrih), emil.zagar@fmf.uni-lj.si (E. Žagar).

https://doi.org/10.1016/j.cam.2026.117987
Received 24 February 2026; Received in revised form 23 June 2026
Available online 22 July 2026

locus, but rather a surface in $\mathbb{H}$. There are infinitely many loci on this surface that generate the given hodograph, and it is necessary to identify which yields the most favourable properties for the spatial PH curve approximant. The basic idea for addressing this issue relies on the fact that any quaternion-valued preimage curve is, up to a sign, in one-to-one correspondence with orthonormal adapted frames associated with the given curve. Recall that the frame is adapted if, at every point on the curve, its first frame vector equals the unit tangent. The alternative L^2 approximation method proposed in this paper is therefore based on selecting, for a given curve, a suitable orthonormal adapted frame and computing its corresponding preimage curve. This preimage curve is then approximated using a linear L^2 approximation scheme by a polynomial or B–spline curve in the preimage space, and the PH approximant is subsequently obtained by well-known operations.

There are several ways to assign an orthonormal adapted frame to a given curve. The Frenet frame is probably the most well-known example. However, for motion design applications, the most suitable adapted frame is the rotation–minimizing frame, which is characterized by the property that its normal frame vectors exhibit no instantaneous rotation about the tangent. Although an analytic expression for this frame is generally not available or difficult to compute, simple algorithms exist for its discrete approximation (e.g., [3]), which are also employed in this paper.

The plan for the rest of this paper is as follows. Section 2 briefly reviews some key properties of spatial PH curves, their preimages, and associated orthonormal frames. Section 3 introduces some basic principles for the approximation of spatial curves by spatial PH curves, based upon a metric for quaternion-valued functions. The full nonlinear L^2 approximation problem is addressed in Section 4, wherein space curves are regarded as pure vector quaternion functions. Section 5 then proposes an alternative approach involving only systems of linear equations, by considering the approximation problem in the quaternion preimage space. Section 6 generalizes these methods from individual polynomial curve segments to the B–spline context. Finally, Section 7 summarizes the principal contributions of this study, and suggest further possible investigations.

2. Spatial Pythagorean–hodograph curves

A spatial Pythagorean–hodograph (PH) curve is a parametric curve $\mathbf{p} : I \subset \mathbb{R} \to \mathbb{R}^3$, $t \mapsto \mathbf{p}(t)$, characterized by the property that its parametric speed $\sigma(t) = |\mathbf{h}(t)|$, $\mathbf{h}(t) := \mathbf{p}'(t)$, which is the derivative $\mathrm{d}s/\mathrm{d}t$ of arc length s with respect to the parameter t, is a *polynomial* in t [1]. The first study [4] of spatial PH curves identified spatial PH cubics in terms of sufficient–and–necessary constraints on their Bézier control polygons, and provided a sufficient algebraic characterization for higher–order spatial PH curves. Subsequently, two alternative sufficient–and–necessary spatial PH curve models, based on the quaternion algebra and the Hopf map from $\mathbb{R}^4$ to $\mathbb{R}^3$, were proposed in [5]. Many algorithms to construct spatial PH curves matching prescribed geometrical data are now available — for example [6–16].

We focus on the quaternion model. A quaternion $\mathcal{Q} = q_0 + q_1\mathbf{i} + q_2\mathbf{j} + q_3\mathbf{k}$ is a four-dimensional number, where q_0, q_1, q_2, q_3 are real values and the basis elements $\mathbf{i}, \mathbf{j}, \mathbf{k}$ satisfy $\mathbf{i}^2 = \mathbf{j}^2 = \mathbf{k}^2 = -1$ and $\mathbf{ij} = \mathbf{k} = -\mathbf{ji}$, $\mathbf{jk} = \mathbf{i} = -\mathbf{kj}$, $\mathbf{ki} = \mathbf{j} = -\mathbf{ik}$. We may write $\mathcal{Q} = (q_0, \mathbf{q})$ where q_0 is the *scalar* part and $\mathbf{q} = q_1\mathbf{i} + q_2\mathbf{j} + q_3\mathbf{k}$ is the *vector* part of $\mathcal{Q}$. The conjugate $\mathcal{Q}^* = (q_0, -\mathbf{q})$ of $\mathcal{Q}$ is such that $\mathcal{Q}\mathcal{Q}^* = \mathcal{Q}^*\mathcal{Q} = |\mathcal{Q}|^2$, where $|\mathcal{Q}| = \sqrt{q_0^2 + q_1^2 + q_2^2 + q_3^2}$ is the modulus of $\mathcal{Q}$. Any non–zero quaternion has an inverse $\mathcal{Q}^{-1} = \mathcal{Q}^*/|\mathcal{Q}|^2$ satisfying $\mathcal{Q}\mathcal{Q}^{-1} = \mathcal{Q}^{-1}\mathcal{Q} = 1$. The sum of quaternions $\mathcal{P} = (p_0, \mathbf{p})$ and $\mathcal{Q} = (q_0, \mathbf{q})$ is simply $\mathcal{P} + \mathcal{Q} = (p_0 + q_0, \mathbf{p} + \mathbf{q})$, and their product may be expressed in terms of the vector dot and cross products as $\mathcal{P}\mathcal{Q} = (p_0 q_0 - \mathbf{p}\cdot\mathbf{q}, p_0\mathbf{q} + q_0\mathbf{p} + \mathbf{p}\times\mathbf{q})$. The following operation $\star : \mathbb{H}\times\mathbb{H} \to \mathbb{R}^3$, defined as

$$\mathcal{P} \star \mathcal{Q} := \tfrac{1}{2}\big(\mathcal{P}\,\mathbf{i}\,\mathcal{Q}^* + \mathcal{Q}\,\mathbf{i}\,\mathcal{P}^*\big),$$

that yields quaternions with a zero scalar part (identified with vectors in $\mathbb{R}^3$), is particularly useful for the construction of PH curves. In particular, when $\mathcal{P} = \mathcal{Q}$, we write $\mathcal{Q} \star \mathcal{Q} =: \mathcal{Q}^{2\star}$. Furthermore, $\sqrt[\star]{\cdot} : \mathbb{R}^3 \setminus \{\mathbf{0}\} \to \mathbb{H}$,

$$\sqrt[\star]{\mathbf{a}} = \begin{cases} \sqrt{|\mathcal{A}|}\,\dfrac{\mathcal{A} + |\mathcal{A}|\mathbf{i}}{|\mathcal{A} + |\mathcal{A}|\mathbf{i}|}, & \mathcal{A} = (0, \mathbf{a}) \neq -\mathbf{i} \\ \sqrt{|\mathcal{A}|}\mathbf{k}, & \text{else} \end{cases} \tag{1}$$

defines the operation that provides a particular solution of the quadratic $\star$–equation $\mathcal{Q}^{2\star} = \mathbf{a}$.

A spatial PH curve is generated from a quaternion *preimage* polynomial $\mathcal{A}(t) = a_0(t) + a_1(t)\,\mathbf{i} + a_2(t)\,\mathbf{j} + a_3(t)\,\mathbf{k}$ by integrating the expression

$$\mathbf{p}'(t) \;=\; \mathcal{A}^{2\star}(t) \;=\; \mathcal{A}(t)\,\mathbf{i}\,\mathcal{A}^*(t)\,. \tag{2}$$

Thus, a quaternion polynomial of degree $\leq m$ implies a PH curve of degree $\leq 2m+1$. The notion of an adapted orthonormal frame, used extensively in this paper, is defined next.

Definition 1. An *adapted* orthonormal frame, associated with a given spatial parametric curve, is a triple of vector-valued functions $(\mathbf{f}_1, \mathbf{f}_2, \mathbf{f}_3)$ such that $\mathbf{f}_1$ is the unit tangent and $\mathbf{f}_2$, $\mathbf{f}_3$ are mutually orthogonal unit vectors spanning the normal plane, at each curve point.

In order to obtain rational adapted orthonormal frames, the spatial curve has to be a PH curve. For a PH curve $\mathbf{p}$ with the hodograph (2), there exists a special adapted orthonormal frame $(\mathbf{e}_1, \mathbf{e}_2, \mathbf{e}_3)$, known as the *Euler–Rodrigues frame* (ERF) [17], defined as

$$\mathbf{e}_1(t) \;=\; \frac{\mathcal{A}(t)\,\mathbf{i}\,\mathcal{A}^*(t)}{|\mathcal{A}(t)|^2}\,, \quad \mathbf{e}_2(t) \;=\; \frac{\mathcal{A}(t)\,\mathbf{j}\,\mathcal{A}^*(t)}{|\mathcal{A}(t)|^2}\,, \quad \mathbf{e}_3(t) \;=\; \frac{\mathcal{A}(t)\,\mathbf{k}\,\mathcal{A}^*(t)}{|\mathcal{A}(t)|^2}\,. \tag{3}$$

Remark 1. For every parameter t, the ERF vectors $\big(\mathbf{e}_1(t), \mathbf{e}_2(t), \mathbf{e}_3(t)\big)$ are identified with the matrix that belongs to a special orthogonal group $SO(3)$. In spatial kinematics, the relation between nonzero quaternions and rotation matrices is known as a kinematic mapping

$$\chi : \mathbb{H} \setminus \{0\} \to \mathrm{SO}(3), \quad \mathcal{Q} \mapsto \chi(\mathcal{Q}) = \tfrac{1}{|\mathcal{Q}|^2}\big(\mathcal{Q}\,\mathbf{i}\,\mathcal{Q}^*, \mathcal{Q}\,\mathbf{j}\,\mathcal{Q}^*, \mathcal{Q}\,\mathbf{k}\,\mathcal{Q}^*\big).$$

Its inverse maps any rotation matrix to two antipodal unit quaternions $\pm\mathcal{Q}$.

One way to compute the inverse of the kinematic mapping is explained in [18]. Another, more suitable, way is given in the following lemma.

Lemma 1. *Let* $\mathbf{O} = (\mathbf{o}_1, \mathbf{o}_2, \mathbf{o}_3) \in \mathrm{SO}(3)$*, and let*

$$\mathcal{Q} = \mathcal{Q}_0\, \mathcal{W}, \tag{4a}$$

where

$$\mathcal{Q}_0 = \sqrt[\star]{\mathbf{o}_1}, \quad \mathcal{W} = \begin{cases} \sqrt{\frac{1+v_3}{2}} + \mathbf{i}\,\frac{v_2}{\sqrt{2(1+v_3)}}, & v_3 \neq -1 \\ 0 + \mathbf{i}, & v_3 = -1 \end{cases}, \quad \text{and} \quad v_\ell = \mathbf{o}_\ell \cdot (\mathcal{Q}_0\,\mathbf{k}\mathcal{Q}_0^*), \quad \ell = 2, 3, \tag{4b}$$

or equivalently,

$$\mathcal{W} = \exp(\phi\,\mathbf{i}) = \cos(\phi) + \sin(\phi)\,\mathbf{i}, \quad \phi \in \left(-\tfrac{\pi}{2}, \tfrac{\pi}{2}\right], \tag{5}$$

for

$$\phi = \begin{cases} \arctan\left(\frac{v_2}{1+v_3}\right), & v_3 \neq -1 \\ \frac{\pi}{2}, & v_3 = -1 \end{cases}.$$

Then $\chi(\pm\mathcal{Q}) = \mathbf{O}$*. This uniquely defined normalized element* $\mathcal{Q} \in \mathbb{H}$ *will be denoted by* $\mathcal{Q} = \mathrm{inv}\chi(\mathbf{O})$*.*

Proof. By the definition of the $\sqrt[\star]{\cdot}$ operation (1), it holds that $\mathbf{o}_1 = \mathcal{Q}_0\,\mathbf{i}\,\mathcal{Q}_0{}^*$. Since $\mathcal{W}\,\mathbf{i}\,\mathcal{W}^* = \mathbf{i}$ for any $\mathcal{W} = \exp(\phi\,\mathbf{i})$ and $\phi \in (-\pi, \pi]$, all solutions $\mathcal{Q}$ of the equation $\mathcal{Q}^{2\star} = \mathbf{o}_1$ equal $\mathcal{Q} = \mathcal{Q}_0\exp(\phi\,\mathbf{i})$. Since we want to compute only one of the two antipodal unit quaternions that are mapped by χ to the matrix $\mathbf{O}$, we limit ϕ to $\left(-\frac{\pi}{2}, \frac{\pi}{2}\right]$, so that $\cos(\phi) \geq 0$. Moreover, it must hold that

$$\mathbf{o}_2 = \mathcal{Q}\,\mathbf{j}\,\mathcal{Q}^* = \cos(2\phi)\,\mathbf{x}_2 + \sin(2\phi)\,\mathbf{x}_3, \quad \mathbf{o}_3 = \mathcal{Q}\,\mathbf{k}\,\mathcal{Q}^* = -\sin(2\phi)\,\mathbf{x}_2 + \cos(2\phi)\,\mathbf{x}_3, \tag{6}$$

where we have denoted $\mathbf{x}_2 = \mathcal{Q}_0\,\mathbf{j}\mathcal{Q}_0^*$ and $\mathbf{x}_3 = \mathcal{Q}_0\,\mathbf{k}\mathcal{Q}_0^*$. Since $|\mathcal{Q}_0| = 1$, also $|\mathbf{x}_2| = |\mathbf{x}_3| = 1$. By applying the vector dot product by $\mathbf{x}_3$ to both equations in (6), and taking into account that $\mathbf{x}_2$ and $\mathbf{x}_3$ are orthogonal, we obtain

$$v_2 = \mathbf{o}_2 \cdot \mathbf{x}_3 = \sin(2\phi), \quad v_3 = \mathbf{o}_3 \cdot \mathbf{x}_3 = \cos(2\phi),$$

where clearly $-1 \leq v_\ell \leq 1$, $\ell = 2, 3$, and $\phi \in \pi\mathbb{Z}$ iff $v_2 = 0$, $v_3 = 1$; $\phi = \frac{\pi}{2} + \pi\mathbb{Z}$ iff $v_2 = 0$, $v_3 = -1$. Using trigonometric identities and the assumption that $\phi \in \left(-\frac{\pi}{2}, \frac{\pi}{2}\right]$, $\phi \neq \frac{\pi}{2}$, these two equations have a unique solution

$$\cos(\phi) = \sqrt{\frac{1+v_3}{2}}, \quad \sin(\phi) = \frac{v_2}{\sqrt{2(1+v_3)}}.$$

If $\phi = \frac{\pi}{2}$, then $v_2 = 0$, $v_3 = -1$ and $\exp(\phi\,\mathbf{i}) = 0 + \mathbf{i}$. This confirms (4). The remaining part follows since $\tan(\phi) = \frac{v_2}{1+v_3}$. □

The inverse of the mapping $\mathbf{p}'(t) = \mathcal{A}^{2\star}(t)$, specified by (2), plays a crucial role in further derivations — i.e., we wish to determine which quaternion-valued functions generate a given Pythagorean hodograph $\mathbf{p}'(t)$. The solution to this problem can by (1) be expressed as

$$\mathcal{K}_{\mathbf{p}}(t,\phi) \;=\; \sqrt[\star]{\mathbf{p}'(t)}\,\exp(\phi\,\mathbf{i}) \;=\; \sqrt{\sigma(t)}\,\frac{\mathbf{p}'(t) + \sigma(t)\,\mathbf{i}}{|\,\mathbf{p}'(t) + \sigma(t)\,\mathbf{i}\,|}\,\exp(\phi\,\mathbf{i})\,, \tag{7}$$

where ϕ is a free angular variable. So, the solution is not a unique quaternion-valued polynomial, but rather a *one-parameter family* of quaternion-valued functions, that defines a two-dimensional *ringed surface* [19–21] in the four-dimensional quaternion space $\mathbb{H}$. For each t, the locus $\mathcal{K}_{\mathbf{p}}(t,\phi)$ is a circle centered on the origin of $\mathbb{H}$. Such an entire circle is the preimage in $\mathbb{H}$ of each hodograph point $\mathbf{p}'(t)$ in $\mathbb{R}^3$.

Remark 2. Assuming that the preimage polynomial $\mathcal{A}(t) = a_0(t) + a_1(t)\,\mathbf{i} + a_2(t)\,\mathbf{j} + a_3(t)\,\mathbf{k}$ of the PH curve $\mathbf{p}(t)$ is known, then from (1) it follows directly that

$$\sqrt[\star]{\mathbf{p}'(t)} \;=\; \sqrt[\star]{\mathcal{A}^{2\star}(t)} \;=\; \tfrac{a_0^2(t)+a_1^2(t)}{\sqrt{a_0^2(t)+a_1^2(t)}}\mathbf{i} + \tfrac{a_1(t)a_2(t)+a_0(t)a_3(t)}{\sqrt{a_0^2(t)+a_1^2(t)}}\mathbf{j} + \tfrac{a_1(t)a_3(t)-a_0(t)a_2(t)}{\sqrt{a_0^2(t)+a_1^2(t)}}\mathbf{k}.$$

This particular solution has zero scalar part. Hence, in order to recover the prescribed preimage polynomial $\mathcal{A}(t)$, it has to be suitably right-multiplied by the factor $\exp(\phi(t)\,\mathbf{i})$. A direct computation shows that the choice

$$\exp(\phi(t)\,\mathbf{i}) = \tfrac{a_1(t)}{\sqrt{a_0^2(t)+a_1^2(t)}} - \tfrac{a_0(t)}{\sqrt{a_0^2(t)+a_1^2(t)}}\mathbf{i}$$

yields $\mathcal{K}_{\mathbf{p}}(t,\phi(t)) \;=\; \mathcal{A}(t)$.

As already noted in the proof of Lemma 1, replacing the preimage $\mathcal{A}(t)$ in (2) by $\mathcal{A}(t)\exp(\phi(t)\,\mathbf{i})$ for any continuous function $\phi(t)$ on the surface (7), leaves the hodograph (2) and hence the unit tangent vector $\mathbf{e}_1(t)$ of the PH curve unchanged, but the normal–plane vectors are transformed to

$$\cos(2\,\phi(t))\,\mathbf{e}_2(t)+\sin(2\,\phi(t))\,\mathbf{e}_3(t) \quad \text{and} \quad -\sin(2\,\phi(t))\,\mathbf{e}_2(t)+\cos(2\,\phi(t))\,\mathbf{e}_3(t),$$

i.e., they are rotated by an angle $2\,\phi(t)$ in the normal plane, at each point $\mathbf{p}(t)$.

The ERF is an important reference frame in identifying rational *rotation–minimizing frames* (RMFs) on spatial PH curves. The RMF consists of the tangent vector and mutually orthogonal normal–plane vectors that exhibit no instantaneous rotation about the tangent. For a certain class of spatial PH curves [22,23], rational RMF normal–plane vectors can be obtained from those of the ERF by means of a certain rational normal–plane rotation. In [20] it was shown that RMFs correspond to choices for $\phi(t)$ that identify *geodesics* on the surface (7). Thus, the RMF can play an important role in the approximation of general space curves by spatial PH curves as described in Section 5.

3. On L^2 approximation of spatial parametric curves

We observe $\mathbb{H}$ as a 4-dimensional vector space over $\mathbb{R}$, and $\mathbb{R}^3=\mathbb{R}\,\mathbf{i}+\mathbb{R}\,\mathbf{j}+\mathbb{R}\,\mathbf{k}$ as its subspace. Consider the vector space $V := C([0,1],\mathbb{H})$ of continuous quaternion-valued functions of a real variable, defined on the interval $[0,1]$. We equip V with the inner product

$$\langle \mathcal{U},\mathcal{V}\rangle=\int_0^1 \tfrac{1}{2}(\mathcal{U}(t)\mathcal{V}^*(t)+\mathcal{V}(t)\,\mathcal{U}^*(t))\,dt=\int_0^1\sum_{i=0}^{3}u_i(t)v_i(t)\,dt, \tag{8}$$

where $\mathcal{U}(t)=u_0(t)\mathbf{1}+u_1(t)\mathbf{i}+u_2(t)\mathbf{j}+u_3(t)\mathbf{k}$, $\mathcal{V}(t)=v_0(t)\mathbf{1}+v_1(t)\mathbf{i}+v_2(t)\mathbf{j}+v_3(t)\mathbf{k}$, and define the *norm* on V as

$$\|\mathcal{U}\|=\sqrt{\langle \mathcal{U},\mathcal{U}\rangle}=\sqrt{\int_0^1 u_0^2(t)+u_1^2(t)+u_2^2(t)+u_3^2(t)\,dt}. \tag{9}$$

Moreover, the distance between two elements $\mathcal{U},\mathcal{V}\in V$ is defined by $\|\mathcal{U}-\mathcal{V}\|$. Note that for the spatial PH curve $\mathbf{r}(t)$, $t\in[0,1]$, defined by integrating (2), the total arc length is $\|\mathcal{A}\|$.

By identifying points $\mathbf{x}=(x,y,z)\in\mathbb{R}^3$ as pure vector quaternions $\mathbf{x}\equiv x\,\mathbf{i}+y\,\mathbf{j}+z\,\mathbf{k}$, with this metric one can define the distance between two spatial parametric curves. In more detail, as any parametric curve can be reparameterized to a fixed interval, we assume throughout the paper that all the curve parameterizations are defined on the interval $[0,1]$. For two curves with regular parameterizations $\mathbf{f}=(f_1,f_2,f_3):[0,1]\to\mathbb{R}^3$ and $\mathbf{g}=(g_1,g_2,g_3):[0,1]\to\mathbb{R}^3$, we define their distance by

$$\operatorname{dist}(\mathbf{f},\mathbf{g}) := \|\mathcal{F}-\mathcal{G}\|=\sqrt{\int_0^1 (f_1(t)-g_1(t))^2+(f_2(t)-g_2(t))^2+(f_3(t)-g_3(t))^2\,dt}, \tag{10}$$

where $\mathcal{F}=f_1\,\mathbf{i}+f_2\,\mathbf{j}+f_3\,\mathbf{k}$, $\mathcal{G}=g_1\,\mathbf{i}+g_2\,\mathbf{j}+g_3\,\mathbf{k}$.

The goal of this paper is to consider the L^2 approximation of given spatial curves by Pythagorean–hodograph curves, where the term L^2 approximation refers to approximation with respect to the distance (10). More generally, choosing a subset $S\subset V$ of the above vector space V, the L^2 approximation problem is to find for every function $\mathcal{F}\in V$ the L^2 approximant $\mathcal{P}\in S$, such that

$$\mathcal{P}=\operatorname*{argmin}_{\mathcal{G}\in S}\|\mathcal{F}-\mathcal{G}\|. \tag{11}$$

If $S\subset V$ is chosen as a finite dimensional subspace there exists a unique solution of (11) for every $\mathcal{F}\in V$, which is computed by solving a linear system of equations (the Gram system). In particular, let $\varphi_\ell:[0,1]\to\mathbb{R}$, $\ell=0,1,\ldots,n$, be linearly independent real–valued functions and let

$$S_4=\operatorname{span}_{\mathbb{R}}\{\varphi_\ell\mathbf{1},\varphi_\ell\mathbf{i},\varphi_\ell\mathbf{j},\varphi_\ell\mathbf{k}\}_{\ell=0}^n\subset V \tag{12}$$

be a $4(n+1)$ dimensional subspace of V, and

$$S_3=\operatorname{span}_{\mathbb{R}}\{\varphi_\ell\mathbf{i},\varphi_\ell\mathbf{j},\varphi_\ell\mathbf{k}\}_{\ell=0}^n\subset V \tag{13}$$

a $3(n+1)$ dimensional subspace of V that contains only the vector-valued functions. Note that $\varphi_\ell\mathbf{1},\varphi_\ell\mathbf{i},\varphi_\ell\mathbf{j},\varphi_\ell\mathbf{k}$ are pairwise orthogonal with respect to the inner product (8) for every ℓ. Any element of S_4 from (12) can be written as

$$\mathcal{G}(t)=\sum_{\ell=0}^{n}\alpha_{\ell,0}\mathbf{1}\varphi_\ell(t)+\alpha_{\ell,1}\mathbf{i}\varphi_\ell(t)+\alpha_{\ell,2}\mathbf{j}\varphi_\ell(t)+\alpha_{\ell,3}\mathbf{k}\varphi_\ell(t)=\sum_{\ell=0}^{n}\mathcal{A}_\ell\varphi_\ell(t),$$

where $\mathcal{A}_\ell=\alpha_{\ell,0}\mathbf{1}+\alpha_{\ell,1}\mathbf{i}+\alpha_{\ell,2}\mathbf{j}+\alpha_{\ell,3}\mathbf{k}\in\mathbb{H}$ for some $\alpha_{\ell,i}\in\mathbb{R}$, and the coefficients that determine for $\mathcal{F}=f_0\mathbf{1}+f_1\mathbf{i}+f_2\mathbf{j}+f_3\mathbf{k}\in V$ its L^2 approximant $\mathcal{P}$ are the solution of

$$\begin{pmatrix}\mathbf{G}&0&0&0\\0&\mathbf{G}&0&0\\0&0&\mathbf{G}&0\\0&0&0&\mathbf{G}\end{pmatrix}\begin{pmatrix}(\alpha_{\ell,0})_{\ell=0}^n\\(\alpha_{\ell,1})_{\ell=0}^n\\(\alpha_{\ell,2})_{\ell=0}^n\\(\alpha_{\ell,3})_{\ell=0}^n\end{pmatrix}=\begin{pmatrix}(\langle\mathcal{F},\varphi_\ell\mathbf{1}\rangle)_{\ell=0}^n\\(\langle\mathcal{F},\varphi_\ell\mathbf{i}\rangle)_{\ell=0}^n\\(\langle\mathcal{F},\varphi_\ell\mathbf{j}\rangle)_{\ell=0}^n\\(\langle\mathcal{F},\varphi_\ell\mathbf{k}\rangle)_{\ell=0}^n\end{pmatrix},$$

where

$$\mathbf{G} = \left(\int_0^1 \varphi_\ell(t)\varphi_{\widetilde{\ell}}(t)\,dt \right)_{\ell,\widetilde{\ell}=0}^{n} \in \mathbb{R}^{(n+1)\times(n+1)}.$$

Since

$$\langle \mathcal{F}, \varphi_\ell \mathbf{1}\rangle = \int_0^1 f_0(t)\,\varphi_\ell(t)\,dt, \quad \left\langle \mathcal{F}, \varphi_\ell\, \mathbf{e}_{\widetilde{\ell}} \right\rangle = \int_0^1 f_{\widetilde{\ell}}(t)\,\varphi_\ell(t)\,dt, \quad \widetilde{\ell} = 1, 2, 3,$$

where we set $\mathbf{e}_1 = \mathbf{i}$, $\mathbf{e}_2 = \mathbf{j}$, $\mathbf{e}_3 = \mathbf{k}$, the Gram system can be written as

$$\mathbf{G}\big(\mathcal{A}_\ell\big)_{\ell=0}^{n} = \left(\int_0^1 \mathcal{F}(t)\varphi_\ell(t)\,dt \right)_{\ell=0}^{n}.$$

Similarly for the vector-valued function $\mathbf{f} \in V$ and S_3 defined in (13), the Gram system determining the L^2 approximant $\sum_{\ell=0}^{n} \mathbf{a}_\ell \varphi_\ell(t)$, $\mathbf{a}_\ell \in \mathbb{R}^3$, is

$$\mathbf{G}\big(\mathbf{a}_\ell\big)_{\ell=0}^{n} = \left(\int_0^1 \mathbf{f}(t)\varphi_\ell(t)\,dt \right)_{\ell=0}^{n}.$$

In what follows, we use for the subspaces S_3 and S_4 the polynomials of some fixed degree $n \in \mathbb{N}_0$, and later the presented construction is generalized to splines equipped with the B–spline basis. We denote by $\mathbb{P}_n = \mathbb{P}_n(\mathbb{R})$, $\mathbb{P}_n(\mathbb{R}^3)$ and $\mathbb{P}_n(\mathbb{H})$ real–valued, vector-valued and quaternion-valued polynomials of degree n in a real variable, respectively. For the basis of $\mathbb{P}_n$ we use the Bernstein basis polynomials, defined by

$$b_\ell^n(t) = \binom{n}{\ell} t^\ell (1-t)^\ell, \quad \ell = 0, 1, \ldots, n.$$

Their Gram matrix $\mathbf{G} = \mathbf{G}_n = \big(g_{i,j}\big)_{i,j=0}^{n}$ has the elements equal to

$$g_{i,j} = \int_0^1 b_i^n(t) b_j^n(t)\,dt = \frac{1}{2n+1} \frac{\binom{n}{i}\binom{n}{j}}{\binom{2n}{i+j}}, \quad i, j = 0, 1, \ldots, n. \tag{14}$$

4. Nonlinear L^2 approximation using spatial Pythagorean–hodograph curves

Let

$$\mathbf{p} : [0,1] \to \mathbb{R}^3 \equiv \mathbb{R}\,\mathbf{i} + \mathbb{R}\,\mathbf{j} + \mathbb{R}\,\mathbf{k}, \quad \mathbf{p}(t) = x(t)\,\mathbf{i} + y(t)\,\mathbf{j} + z(t)\,\mathbf{k},$$

be a spatial polynomial PH curve, constructed from the preimage polynomial $\mathcal{A} \in \mathbb{P}_m(\mathbb{H})$ by the integration $\mathbf{p}(t) = \int_0^t \mathbf{h}(u)\,du + \mathbf{p}_0$ of the hodograph $\mathbf{h} = \mathcal{A}^{2\star} \in \mathbb{P}_{2m}(\mathbb{R}^3)$. Here $\mathbf{p}_0 \in \mathbb{R}^3$ is a free integration constant. Denoting

$$\mathcal{A}(t) = \sum_{\ell=0}^{m} \mathcal{A}_\ell\, b_\ell^m(t), \quad \mathcal{A}_\ell = \alpha_{\ell,0}\,\mathbf{1} + \alpha_{\ell,1}\,\mathbf{i} + \alpha_{\ell,2}\,\mathbf{j} + \alpha_{\ell,3}\,\mathbf{k} \in \mathbb{H}, \tag{15}$$

the hodograph is

$$\mathbf{h}(t) = \sum_{\ell=0}^{2m} \mathbf{h}_\ell\, b_\ell^{2m}(t), \quad \mathbf{h}_\ell = h_{\ell,1}\,\mathbf{i} + h_{\ell,2}\,\mathbf{j} + h_{\ell,3}\,\mathbf{k}, \tag{16}$$

where

$$\mathbf{h}_\ell = \sum_{\widetilde{\ell}=\max(0,\ell-m)}^{\min(m,\ell)} \frac{\binom{m}{\widetilde{\ell}}\binom{m}{\ell-\widetilde{\ell}}}{\binom{2m}{\ell}} \mathcal{A}_{\widetilde{\ell}} \star \mathcal{A}_{\ell-\widetilde{\ell}}, \quad \ell = 0, 1, \ldots, 2m, \tag{17}$$

and

$$\mathbf{p}(t) = \sum_{\ell=0}^{2m+1} \mathbf{p}_\ell b_\ell^{2m+1}(t), \quad \mathbf{p}_\ell = p_{\ell,1}\,\mathbf{i} + p_{\ell,2}\,\mathbf{j} + p_{\ell,3}\,\mathbf{k}, \tag{18}$$

where

$$\mathbf{p}_{\ell+1} = \mathbf{p}_\ell + \frac{1}{2m+1}\mathbf{h}_\ell, \quad \ell = 0, 1, \ldots, 2m. \tag{19}$$

As the multiplication of $\mathcal{A}(t)$ by $\exp(\phi\,\mathbf{i})$ for any constant $\phi \in \left(-\frac{\pi}{2}, \frac{\pi}{2}\right]$ keeps the degree of $\mathcal{A}(t)$ unchanged and does not change the hodograph, we can fix $\mathrm{scal}(\mathcal{A}_0) = 0$. Thus, a spatial PH curve of odd degree $n = 2m+1$ has $4(m+1) - 1 + 3 = 4m + 6$ degrees of freedom. Let

$$\mathcal{PH}_n = \left\{ \mathbf{p} : [0,1] \to \mathbb{R}^3;\ \mathbf{p}' = \mathcal{A}^{2\star} \text{ for some } \mathcal{A} \in \mathbb{P}_m(\mathbb{H}),\ m = (n-1)/2,\ \mathrm{scal}(\mathcal{A}(0)) = 0 \right\}$$

be the set of spatial PH curves of odd degree n. For any given $\mathbf{f} = f_1\,\mathbf{i} + f_2\,\mathbf{j} + f_3\,\mathbf{k} \in C([0,1],\mathbb{R}^3)$, finding its L^2–PH approximant in $\mathcal{PH}_n$ incurs the nonlinear optimization problem

$$\min_{\mathbf{p}\in\mathcal{PH}_n} \|\mathbf{f}-\mathbf{p}\|^2 = \tag{20}$$
$$\min_{\mathbf{p}\in\mathcal{PH}_n} \left\{ \int_0^1 (f_1(t)-x(t))^2 + (f_2(t)-y(t))^2 + (f_3(t)-z(t))^2\,dt;\ \mathbf{p}(t) = x(t)\,\mathbf{i} + y(t)\,\mathbf{j} + z(t)\,\mathbf{k} \right\},$$

where the norm is defined in (9). By (18) the curve $\mathbf{p}$ is uniquely determined by the coefficients $\mathcal{A}_\ell \in \mathbb{H}$, $\ell = 0,1,\ldots,m$, with $\mathrm{scal}(\mathcal{A}_0) = 0$, and $\mathbf{p}_0 \in \mathbb{R}^3$. Moreover, from (17) and (19) we see that the control points $\mathbf{p}_\ell$ depend nonlinearly on the coefficients of the preimage. Solving the minimization problem (20) is thus equivalent to finding the minimum of the nonlinear function Ψ of $4m+6$ real variables defined by

$$\Psi(\mathcal{A}_0,\ldots,\mathcal{A}_m,\mathbf{p}_0) = \Psi(\alpha_{0,1},\alpha_{0,2},\alpha_{0,3},(\alpha_{\ell,0},\alpha_{\ell,1},\alpha_{\ell,2},\alpha_{\ell,3})_{\ell=1}^m,p_{0,1},p_{0,2},p_{0,3}) :=$$
$$\int_0^1 (f_1(t)-x(t))^2 + (f_2(t)-y(t))^2 + (f_3(t)-z(t))^2\,dt.$$

This may be further simplified to

$$\Psi(\mathcal{A}_0,\ldots,\mathcal{A}_m,\mathbf{p}_0) = \sum_{i,j=0}^n \left(\sum_{k=1}^3 p_{i,k}p_{j,k}\right) g_{i,j} - 2\sum_{i=0}^n\sum_{k=1}^3 p_{i,k}\gamma_{i,k} + \gamma, \tag{21}$$

where $g_{i,j}$ are given in (14) and

$$\gamma_{i,k} = \int_0^1 f_k(t)b_i^n(t)\,dt, \quad \gamma = \int_0^1 f_1^2(t) + f_2^2(t) + f_3^2(t)\,dt. \tag{22}$$

Note that $g_{i,j}$ satisfy $\sum_{j=0}^n g_{i,j} = \frac{1}{n+1}$. The problem can be solved by some nonlinear optimization solver or a Newton–Raphson iteration applied to the nonlinear system of $4m+6$ equations

$$\frac{\partial\Psi}{\partial\alpha_{0,1}} = \frac{\partial\Psi}{\partial\alpha_{0,2}} = \frac{\partial\Psi}{\partial\alpha_{0,3}} = 0,\ \frac{\partial\Psi}{\partial\alpha_{\ell,k}} = 0,\ k=0,\ldots,3,\ \ell=1,\ldots,m,\ \frac{\partial\Psi}{\partial p_{0,1}} = \frac{\partial\Psi}{\partial p_{0,2}} = \frac{\partial\Psi}{\partial p_{0,3}} = 0.$$

In both cases, the convergence of the iterative procedure and the resulting solution depend significantly on the choice of the initial values. This motivates the development of a simpler alternative approach that requires solving a linear system of equations.

5. Alternative L^2 approximation using spatial Pythagorean–hodograph curves

We now propose an alternative approach to construct the PH curve that approximates a given $\mathbf{f} : [0,1] \to \mathbb{R}^3$ and is close to the nonlinear L^2–PH approximant from $\mathcal{PH}_n$, described in the previous section. We assume that $\mathbf{f} \in C^1([0,1];\mathbb{R}^3)$ and has non-vanishing first order derivatives. As in [2], the basic idea is to make the problem linear by performing the standard linear L^2 approximation in the preimage space rather than directly in $\mathcal{PH}_n$.

As noted in Section 2, even if $\mathbf{f}$ itself is a spatial PH curve, it admits infinitely many preimages, that lie on the surface (7). If $\mathbf{f}$ is not a PH curve, then its preimage is any quaternion-valued function $\mathcal{A}_\mathbf{f}$, such that

$$\mathbf{f}' = \mathcal{A}_\mathbf{f}^{2\star}.$$

Again, there exist infinitely many such preimages, and each of them defines, via (3), an orthonormal adapted frame. The converse also holds. Therefore, the idea is to equip $\mathbf{f}$ with a chosen orthonormal adapted frame $\mathbf{O} = (\mathbf{o}_1,\mathbf{o}_2,\mathbf{o}_3)$ and compute the preimage curve in the following way.

Definition 2. For $\mathbf{f} \in C^1([0,1];\mathbb{R}^3)$ with non-vanishing first order derivatives and a chosen orthonormal adapted frame $\mathbf{O} = (\mathbf{o}_1,\mathbf{o}_2,\mathbf{o}_3)$, the preimage curve is defined as

$$\mathcal{A}_\mathbf{f}(t) = \varsigma(t)\sqrt{|\mathbf{f}'(t)|}\,\mathrm{inv}\chi(\mathbf{O}(t)), \quad t \in [0,1],$$

where $\mathrm{inv}\chi$ is given in Lemma 1, and function $\varsigma : [0,1] \to \{-1,1\}$, $\varsigma(0) = 1$, controls the sign in a way that makes $\mathcal{A}_\mathbf{f}$ continuous.

It remains to investigate how one can assign, for any given non–PH curve $\mathbf{f}$, an orthonormal adapted frame that yields a "good" curve in the preimage space. Probably the most well–known orthonormal frame that can be assigned to a C^2 parametric curve $\mathbf{f}$ with non–zero $\mathbf{f}'(t)\times\mathbf{f}''(t)$ for $t \in [0,1]$ is the Frenet frame, which consists of the three vector-valued functions $(\mathbf{t},\mathbf{n},\mathbf{b})$,

$$\mathbf{t} = \frac{\mathbf{f}'}{|\mathbf{f}'|}, \quad \mathbf{n} = \frac{\mathbf{f}'\times\mathbf{f}''}{|\mathbf{f}'\times\mathbf{f}''|}\times\mathbf{t}, \quad \mathbf{b} = \frac{\mathbf{f}'\times\mathbf{f}''}{|\mathbf{f}'\times\mathbf{f}''|}, \tag{23}$$

defining three orthonormal vectors at each point of the curve $\mathbf{f}(t)$: the unit tangent vector $\mathbf{t}(t)$, the principal normal vector $\mathbf{n}(t)$, and the binormal vector $\mathbf{b}(t)$. Furthermore, as observed in Section 2, the *rotation–minimizing frame* (RMF) on a spatial PH curve corresponds to a "simple" curve — a geodesic — on the surface (7). This reflects the fact that the derivatives of the RMF normal–plane vectors are always aligned with the tangent — they vary only because they are constrained to lie in the normal plane at each point. This suggests that the RMF should also be a good choice for an orthonormal adapted frame on the non–PH curve $\mathbf{f}$. However, its analytical computation is quite complicated. The deviation of the RMF from the Frenet frame is specified in [24] and includes the computation of the integral of the torsion with respect to arc length. This integral has an analytic reduction for spatial PH curves [25], but in general there is no such reduction for non–PH curves. However, there are many algorithms that provide discrete approximations to the RMF. Here we adopt the *double reflection method* proposed in [3], and described in Algorithm 1. An important advantage of this method is that it requires only a sequence of points on the curve together with the corresponding unit tangent vectors, and therefore can be applied to curves that are merely C^1. The method is based on the following iterative construction. Given two consecutive data points $\mathbf{P}_0$, $\mathbf{P}_1$ with unit tangents $\mathbf{t}_0$, $\mathbf{t}_1$, and an initial orthonormal frame $(\mathbf{t}_0, \mathbf{r}_0, \mathbf{s}_0)$, the next frame $(\mathbf{t}_1, \mathbf{r}_1, \mathbf{s}_1)$ is obtained by two successive reflections. First, the vectors $\mathbf{r}_0$ and $\mathbf{t}_0$ are reflected across the bisector plane of the segment joining $\mathbf{P}_0$ and $\mathbf{P}_1$, yielding intermediate vectors $\mathbf{r}_0^L$ and $\mathbf{t}_0^L$. The vector $\mathbf{r}_0^L$ is then reflected across the bisector plane of the segment joining $\mathbf{P}_1 + \mathbf{t}_0^L$ and $\mathbf{P}_1 + \mathbf{t}_1$, producing the vector $\mathbf{r}_1$ and hence the frame $(\mathbf{t}_1, \mathbf{r}_1, \mathbf{t}_1 \times \mathbf{r}_1)$. The reflections are implemented via Householder transformations, making the method computationally efficient. As shown in [3], the method is exact for spherical curves and achieves fourth-order accuracy for general curves.

Algorithm 1 Computation of rotation minimizing frame vectors.

Input: sequence of data points $\mathbf{P}_j$ and unit tangent vectors $\mathbf{t}_j$ $j = 0, 1, \ldots, J$.
$\mathcal{Q}_0 = \sqrt[\star]{\mathbf{t}_0}$
$(\mathbf{r}_0, \mathbf{s}_0) = (\mathcal{Q}_0 \mathbf{j} \mathcal{Q}_0^*, \mathcal{Q}_0 \mathbf{k} \mathcal{Q}_0^*)$
$\mathbf{O}_0 = (\mathbf{t}_0, \mathbf{r}_0, \mathbf{s}_0)$
`for` $j = 0, 1, \ldots, J-1$
  $\mathbf{v}_1 = \mathbf{P}_{j+1} - \mathbf{P}_j$
  $c_1 = \mathbf{v}_1 \cdot \mathbf{v}_1$
  $\mathbf{r}_j^L = \mathbf{r}_j - \frac{2}{c_1}(\mathbf{v}_1 \cdot \mathbf{r}_j)\mathbf{v}_1$
  $\mathbf{t}_j^L = \mathbf{t}_j - \frac{2}{c_1}(\mathbf{v}_1 \cdot \mathbf{t}_j)\mathbf{v}_1$
  $\mathbf{v}_2 = \mathbf{t}_{j+1} - \mathbf{t}_j^L$
  $c_2 = \mathbf{v}_2 \cdot \mathbf{v}_2$
  $\mathbf{r}_{j+1} = \mathbf{r}_j^L - \frac{2}{c_2}(\mathbf{v}_2 \cdot \mathbf{r}_j^L)\mathbf{v}_2$
  $\mathbf{s}_{j+1} = \mathbf{t}_{j+1} \times \mathbf{r}_{j+1}$
  $\mathbf{O}_{j+1} = (\mathbf{t}_{j+1}, \mathbf{r}_{j+1}, \mathbf{s}_{j+1})$
`end for`
Output: $\mathbf{O}_j$, $j = 0, 1, \ldots, J$.

The algorithm takes as input a sequence of points and unit tangents of the given parametric curve $\mathbf{f}$. In particular, let $t_0 = 0 < t_1 < \cdots < t_{J-1} < t_J = 1$ for some sufficiently large $J \in \mathbb{N}$ be a chosen sequence of equidistant parameter values. Since the double reflection method is fourth-order accurate, the results are relatively insensitive to the precise choice of J once a sufficiently fine discretization is used. However, the required level of discretization depends on the geometric complexity of the curve under consideration. Let $\mathbf{P}_j = \mathbf{f}(t_j)$, $\mathbf{t}_j = \mathbf{f}'(t_j)/|\mathbf{f}'(t_j)|$ be the corresponding sequence of data points together with unit tangents. By applying Algorithm 1, we obtain a sequence of $SO(3)$ matrices (orthonormal vectors)

- `Method` 1 (RMF): $\mathbf{O}_j = (\mathbf{o}_{j,1}, \mathbf{o}_{j,2}, \mathbf{o}_{j,3})$, $j = 0, 1 \ldots, J$,

and we call this choice `Method` 1. The following two choices will also be considered:

- `Method` 2 (Frenet frame (23)): $\mathbf{O}_j = (\mathbf{t}(t_j), \mathbf{n}(t_j), \mathbf{b}(t_j))$, $j = 0, 1 \ldots, J$,
- `Method` 3: $\mathbf{O}_j = (\mathcal{X}_j\, \mathbf{i}\, \mathcal{X}_j{}^*, \mathcal{X}_j\, \mathbf{j}\, \mathcal{X}_j{}^*, \mathcal{X}_j\, \mathbf{k}\, \mathcal{X}_j{}^*)$, $\mathcal{X}_j = \mathcal{K}_{\mathbf{f}}(t_j, 0) = \sqrt[\star]{\mathbf{t}(t_j)}$, $j = 0, 1 \ldots, J$.

Using the inverse $\mathrm{inv}\chi$ of the kinematic mapping χ, provided by Lemma 1, we compute the unit quaternions

$$\widetilde{\mathcal{Q}}_j = \varsigma_j\, \mathrm{inv}\chi(\mathbf{O}_j) = \varsigma_j \sqrt[\star]{\mathbf{o}_{j,1}}\, \mathcal{W}_j \in \mathbb{H}, \quad j = 0, 1, \ldots, J, \tag{24a}$$

where $\varsigma_0 = \varsigma(0) = 1$, and for $j \geq 1$ the sign $\varsigma_j = \varsigma(t_j) \in \{-1, 1\}$ is chosen so that the two neighbouring quaternions lie on the same side of the unit quaternion sphere (the inner product of two consecutive $\mathcal{Q}_j$ and $\mathcal{Q}_{j+1}$ is nonnegative). We incorporate the sign into $\mathcal{W}_j$, i.e., we replace $\mathcal{W}_j$ by $\varsigma_j\, \mathcal{W}_j$. Furthermore, we set

$$\mathcal{Q}_j = \sqrt{|\mathbf{f}'(t_j)|}\, \sqrt[\star]{\mathbf{o}_{j,1}}\, \mathcal{W}_j = \sqrt[\star]{\mathbf{f}'(t_j)}\, \mathcal{W}_j, \quad j = 0, 1, \ldots, J, \tag{24b}$$

and we use this sequence of quaternions as the values of the preimage curve $\mathcal{A}_{\mathbf{f}}$ at parameters t_j, i.e., $\mathcal{A}_{\mathbf{f}}(t_j) = \mathcal{Q}_j$.

Although the computation of the preimage curve is presented for a discrete set of parameter values, it can be straightforwardly extended to a continuous setting for `Method` 2 and `Method` 3. This extension is particularly simple for `Method` 3, since $\mathcal{W}$ and ς are identically equal to 1. For `Method` 2, locating the jumps of the function ς requires determining the parameter values for which $v_3 = -1$ and v_2 changes sign, where v_2 and v_3 are defined in Lemma 1 and observed here as functions of the parameter t.

Another way to define $\mathcal{A}_{\mathbf{f}}$ on the whole interval $[0,1]$ is to interpolate the values (24b) by a piecewise-linear function, defined as

$$\mathcal{A}_{\mathbf{f}}(t) = \sqrt[4]{\mathbf{f}'(t)}\,\mathcal{W}(t), \quad \mathcal{W}\Big|_{[t_j,t_{j+1}]}(t) = \frac{\mathcal{W}_j \frac{t_{j+1}-t}{t_{j+1}-t_j} + \mathcal{W}_{j+1}\frac{t-t_j}{t_{j+1}-t_j}}{\left|\mathcal{W}_j \frac{t_{j+1}-t}{t_{j+1}-t_j} + \mathcal{W}_{j+1}\frac{t-t_j}{t_{j+1}-t_j}\right|}, \quad j = 0,1\ldots,J-1. \tag{24c}$$

Once the preimage $\mathcal{A}_{\mathbf{f}} : [0,1] \to \mathbb{H}$ is determined, the alternative L^2 PH approximant is constructed as described in Algorithm 2.

Algorithm 2 Alternative–L^2–PH approximant.

Input: $\mathbf{f} \in \mathcal{C}^1([0,1],\mathbb{R}^3)$, preimage $\mathcal{A}_{\mathbf{f}} : [0,1] \to \mathbb{H}$, degree m
1: compute $\mathbf{G}_m = \left(\left\langle b_\ell^m, b_k^m \right\rangle\right)_{k,\ell=0}^m \in \mathbb{R}^{(m+1)\times(m+1)}$ by (14)
2: compute $\mathbf{g} = \left(\left\langle \mathcal{A}_{\mathbf{f}}, b_\ell^m \right\rangle\right)_{\ell=0}^m \in \mathbb{H}^{m+1}$
3: solve the Gram system $\mathbf{G}\big(\mathcal{A}_\ell\big)_{\ell=0}^m = \mathbf{g}$ for unknowns $(\mathcal{A}_\ell)_{\ell=0}^m \in \mathbb{H}^{m+1}$
4: define the preimage as in (15)
5: compute the hodograph (16)
6: choose $\mathbf{p}_0$
7: determine $\mathbf{p}$ by (18)
Output: PH curve $\mathbf{p}$

The second step of Algorithm 2 includes the computation of integrals, which in general can not be computed analytically. In numerical computations, the integrals are approximated using some quadrature rule that needs only the function values over the chosen sequence of integration knots. In what follows, we propose to choose the composite Simpson rule with knots $(t_j)_{j=0}^J$, $t_j = jh$, $h = \frac{1}{J}$, for an even number $J \in \mathbb{N}$:

$$\int_0^1 f(t)\,dt \approx I_h(f) := \frac{h}{3}\left(f(0) + 4\sum_{j=0}^{(J-2)/2} f(t_{2j+1}) + 2\sum_{j=1}^{(J-2)/2} f(t_{2j}) + f(1)\right).$$

Note that the error of this quadrature for smooth functions equals $\mathcal{O}(h^4) = \mathcal{O}(J^{-4})$. Thus, in numerical computations the elements of the vector $\mathbf{g} = (g_\ell)_{\ell=0}^m$ are computed as $g_\ell = I_h(\mathcal{A}_{\mathbf{f}}\, b_\ell^m)$.

It remains to explain how to choose the integration constant and the point $\mathbf{p}_0$ in step 6 of the algorithm. As in the case of planar curves (see [2, Section 4]) we propose to compute $\mathbf{p}_0$ so that

$$\mathbf{p}_0^* = \underset{\mathbf{p}_0\in\mathbb{R}^3}{\operatorname{argmin}} \|\mathbf{f} - \mathbf{p}\|,$$

where $\mathbf{p}' = \mathcal{A}^{2\star}$ for $\mathcal{A}$ computed in step 4 of Algorithm 2. Since this is a linear problem, we obtain by some straightforward computations that

$$\mathbf{p}_0^* = \sum_{j=0}^n (\gamma_{j,k})_{k=1}^3 - \frac{1}{n(n+1)}\sum_{j=1}^n\sum_{\ell=0}^{j-1} \mathbf{h}_\ell, \tag{25}$$

where the notation from (22) is employed. With this choice, the resulting curve of degree $n = 2m+1$ is called the *alternative* L^2 PH approximant. Note that this curve depends on the chosen method for computing the orthonormal frame. If $\mathbf{f}$ is itself a PH curve, and its preimage polynomial is known, choosing this polynomial as $\mathcal{A}_{\mathbf{f}}$ reproduces the curve using the proposed alternative method, as revealed in the next remark.

Remark 3. Suppose that $\mathbf{f}$ is a PH curve of degree $2m+1$ computed from the preimage curve $\widetilde{\mathcal{A}} \in \mathbb{P}_m(\mathbb{H})$. Then the alternative L^2 PH approximant reproduces $\mathbf{f}$ provided that one chooses $\mathcal{A}_{\mathbf{f}} = \widetilde{\mathcal{A}}$ and $\mathbf{p}_0$ by (25). Namely, from the uniqueness of the solution of the Gram system and the fact that $\widetilde{\mathcal{A}}$ lies in the subspace $\mathbb{P}_m(\mathbb{H})$, it follows that the preimage $\mathcal{A}$ computed in steps 3–4 of Algorithm 2 satisfies $\mathcal{A} = \widetilde{\mathcal{A}}$. Furthermore

$$\min_{\mathbf{p}_0\in\mathbb{R}^3} \|\mathbf{f}-\mathbf{p}\| = \min_{\mathbf{p}_0\in\mathbb{R}^3} \left\| \int_0^t \widetilde{\mathcal{A}}^{2\star}(u)\,du + \mathbf{f}(0) - \left(\int_0^u \mathcal{A}^{2\star}(u)\,du + \mathbf{p}_0\right)\right\| = \min_{\mathbf{p}_0\in\mathbb{R}^3}\|\mathbf{f}(0)-\mathbf{p}_0\|,$$

so clearly $\mathbf{p}_0 = \mathbf{f}(0)$, which confirms the statement. Note that, if $\mathcal{A}_{\mathbf{f}}$ is computed by (24) using some frame other than the ERF of the original PH curve, then $\mathbf{f}$ is not necessarily reproduced. If the preimage polynomial of a spatial PH curve $\mathbf{f}$ is not given, determining it is known as the reverse-engineering problem for PH curves. Explicit solutions for cubic and quintic PH curves are given in [26]. For arbitrary degrees, constructive frameworks based on rational motions and quaternion-polynomial factorization have been developed in [27,28].

We now demonstrate the presented construction by several numerical examples. In addition to the *alternative* L^2–PH approximants, we also compute the *nonlinear* approximants introduced in Section 4. Specifically, using the preimage Bézier coefficients and $\mathbf{p}_0$ of the alternative L^2–PH approximant as initial values for the optimization solver (which is used to compute the minimum of a function (21)),

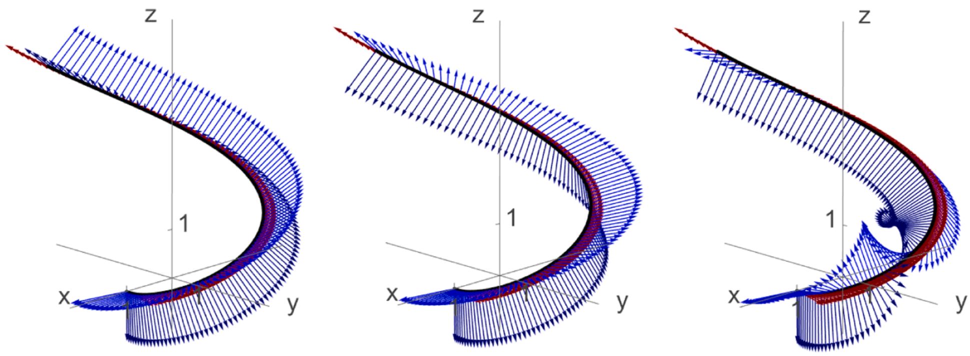

Fig. 1. Curve $\mathbf{f}$ equipped with orthonormal frames computed by `Method 1` (left), `Method 2` (middle) and `Method 3` (right). The plotted vectors correspond to equidistant parameter values with step size $1/100$.

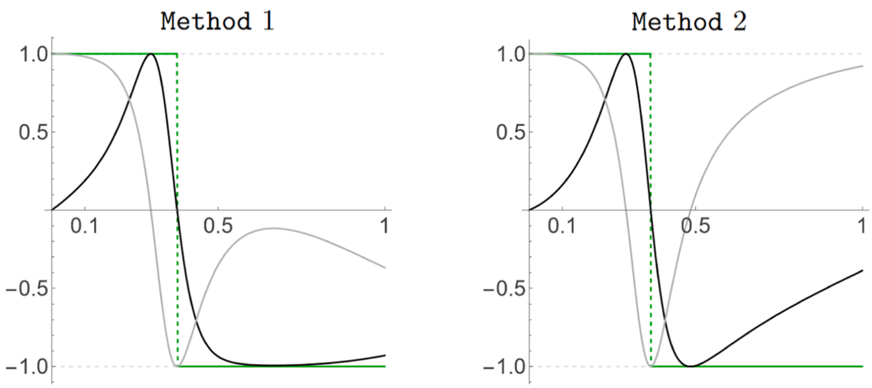

Fig. 2. Graphs of functions v_2 (black) and v_3 (gray) that determine $\mathcal{W}$ by (4), and the sign function ς (green), used in (24a), for methods `Method 1` and `Method 2`.

provides an effective procedure for computing the nonlinear L^2–PH approximants. However, as is typical for nonlinear problems, the iterations may converge to a local rather than a global minimum. When different initial values yield distinct approximants, the one with the smallest objective function value (21) is chosen.

To measure the quality of the computed approximants and their associated ER frames, we observe the L^2 distance, defined by (10), and

$$\mathrm{E}_{\omega}(\mathcal{A}) := \int_0^1 \omega_1^2(t)\,dt, \quad \omega_1 := \mathbf{e}_2 \cdot \mathbf{e}_3',$$

which measures the amount of rotation of the ER frame vectors $\mathbf{e}_2$ and $\mathbf{e}_3$ (defined by (3) for the computed preimage $\mathcal{A}$), around the tangent $\mathbf{e}_1$. Note that E_{ω} equals zero if the frame is rotation–minimizing.

Example 1. Consider the curve

$$\mathbf{f}(t) = \left(e^t \cos(5t), e^t \sin(5t), 10\sqrt{t^2+1} - 10\right), \quad t \in [0,1] \tag{26}$$

for which we compare the alternative L^2–PH approximants computed using three different methods, `Method 1`, `Method 2`, and `Method 3`, to equip $\mathbf{f}$ with an orthonormal frame. The numerical computations are performed discretely over a sequence of equidistant parameters $t_j = j/J$, $j = 0, 1, \ldots, J$, where $J = 500$. Note that at $t = 0$ the frame vectors obtained by `Method 1` and `Method 3` coincide. Since this is not true in general for the Frenet frame, we rotate it about $\mathbf{e}_1$ so that the initial orientations coincide for all three methods. The computed frames are shown in Fig. 1. One can observe that `Method 3`, although the simplest, yields poor results, as the normal-plane frame vectors exhibit a large amount of undesirable rotation about the tangent. Recall that, in the computation of $\mathrm{inv}\mathcal{X}$, we take $\mathcal{W} \equiv 1$ and $\varsigma \equiv 1$ for the `Method 3`. For `Method 1` and `Method 2`, graphs of functions v_2 and v_3 (defined in Lemma 1) that determine $\mathcal{W}$, together with the sign function ς are shown in Fig. 2, confirming our theoretical statements.

Choosing $m = 2$ as the degree of the preimage polynomial $\mathcal{A}(t)$, we obtain the following results for its Bernstein coefficients and the initial point $\mathbf{p}_0$.

`Method 1 :`

$$\mathcal{A}_0 = 0.023654 + 2.0993\mathbf{i} + 1.4331\mathbf{j} - 0.26166\mathbf{k}, \quad \mathcal{A}_1 = -0.49815 - 1.2590\mathbf{i} + 4.3481\mathbf{j} + 1.9431\mathbf{k},$$

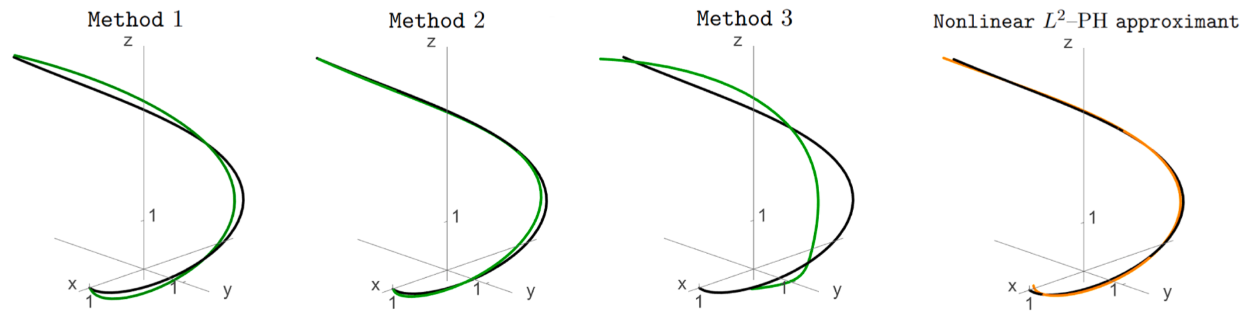

Fig. 3. Graph of the original curve (26) (black) together with quintic alternative L^2–PH approximants for all three used methods (green; first three figures), and the quintic nonlinear L^2–PH approximant (orange; last figure).

Table 1
The L^2 distances between the curve $\mathbf{f}$ defined in (26) and its alternative and nonlinear L^2–PH approximants (from Example 1) for different degrees $n = 2m + 1$, $m = 1, 2, \dots, 5$, together with values of the functional E_ω.

	Method 1		Method 2	
m	dist	E_ω	dist	E_ω
1	$5.7012 \cdot 10^{-1}$	$1.0066 \cdot 10^{0}$	$5.4653 \cdot 10^{-1}$	2.3030
2	$1.3191 \cdot 10^{-1}$	$3.6991 \cdot 10^{-1}$	$1.0940 \cdot 10^{-1}$	3.1389
3	$2.5289 \cdot 10^{-2}$	$6.4483 \cdot 10^{-2}$	$1.4215 \cdot 10^{-2}$	3.2741
4	$4.3394 \cdot 10^{-3}$	$1.5525 \cdot 10^{-2}$	$2.0389 \cdot 10^{-3}$	3.1323
5	$6.4543 \cdot 10^{-4}$	$3.6536 \cdot 10^{-4}$	$2.9173 \cdot 10^{-4}$	3.1065
	Method 3		nonlinear	
m	dist	E_ω	dist	E_ω
1	$1.3942 \cdot 10^{0}$	$4.1896 \cdot 10^{0}$	$3.3175 \cdot 10^{-1}$	1.2577
2	$6.4717 \cdot 10^{-1}$	$2.3818 \cdot 10^{1}$	$5.1580 \cdot 10^{-2}$	2.1791
3	$4.1479 \cdot 10^{-1}$	$3.5636 \cdot 10^{1}$	$4.2277 \cdot 10^{-3}$	3.9774
4	$2.0392 \cdot 10^{-1}$	$4.2981 \cdot 10^{1}$	$2.4637 \cdot 10^{-4}$	2.8239
5	$1.4124 \cdot 10^{-1}$	$4.6326 \cdot 10^{1}$	$1.2627 \cdot 10^{-5}$	2.8128

$$\mathcal{A}_2 = -3.3962 - 2.4768 + 0.47012\mathbf{j} - 0.39784\mathbf{k}, \quad \mathbf{p}_0 = (1.0056, 0.029750, 0.000051481)$$

`Method 2 :`

$$\mathcal{A}_0 = 0.17139 + 2.0480\mathbf{i} + 1.2777\mathbf{j} + 0.095688\mathbf{k}, \quad \mathcal{A}_1 = -1.3435 - 0.88202\mathbf{i} + 4.8920\mathbf{j} + 0.83261\mathbf{k},$$

$$\mathcal{A}_2 = -0.85450 - 4.1395\mathbf{i} + 0.053688\mathbf{j} - 1.0915\mathbf{k}, \quad \mathbf{p}_0 = (1.0122, 0.040170, 0.0034594)$$

`Method 3 :`

$$\mathcal{A}_0 = 1.5397\mathbf{i} + 3.6065\mathbf{j} + 0.036315\mathbf{k}, \quad \mathcal{A}_1 = -0.38170\mathbf{i} - 4.3725\mathbf{j} + 3.6234\mathbf{k},$$

$$\mathcal{A}_2 = 4.5744\mathbf{i} - 0.28975\mathbf{j} + 0.15485\mathbf{k}, \quad \mathbf{p}_0 = (0.67124, -0.16915, -0.26002).$$

Graphs of the alternative L^2–PH approximants are shown in Fig. 3 (green curves). The orange curves also show the nonlinear L^2–PH approximant, presented in Section 4, which is computed by the minimization of (21) with initial values obtained from the alternative approximants (rotated in such a way that the scalar part of $\mathcal{A}_0$ equals zero as required). Table 1 shows the L^2 distance between $\mathbf{f}$ and its alternative L^2–PH approximants for all three methods, as well as the L^2 distance between $\mathbf{f}$ and its nonlinear L^2–PH approximants for different degrees $n = 2m + 1$, $m = 1, 2, \dots, 5$. The values of the functional E_ω are also listed, allowing comparison of the quality of the ER frames.

Example 2. We now explore the asymptotic behaviour of the alternative L^2–PH approximants and their nonlinear counterparts, based on successively smaller segments of the curve (26). Specifically, we approximate the sequence of curves $\mathbf{f}_h(t) := \mathbf{f}(th)$ for $h = 1/2^k$, $k = 0, 1, \dots, 5$, and $t \in [0, 1]$, with preimage curves computed using `Method 1` and `Method 2` with $J = 500$. The results shown in Table 2 for degree $m = 1$ and in Table 3 for degree $m = 2$ indicate that the approximation order is $m + 2$ for the alternative as well as the nonlinear L^2–PH approximant.

Example 3. Consider a PH curve $\mathbf{f}$ of degree 9, generated from a preimage polynomial $\mathcal{A}$ of degree 4 with Bernstein coefficients and initial point $\mathbf{p}_0$ specified by

$$\mathcal{A}_0 = 2\mathbf{i} + \tfrac{3}{2}\mathbf{j}, \quad \mathcal{A}_1 = -2 + \mathbf{i} + 3\mathbf{j} + \tfrac{1}{2}\mathbf{k}, \quad \mathcal{A}_2 = -1 - 1\mathbf{i} + 4\mathbf{j} + \tfrac{1}{2}\mathbf{k},$$

Table 2
The L^2 distances between $\mathbf{f}_h$, where $\mathbf{f}$ is defined in (26), and cubic ($m = 1$) alternative L^2 PH approximants (obtained by `Method` 1 and `Method` 2) and the nonlinear one, together with decay exponents (estimated approximation orders).

	Method 1		Method 2		nonlinear	
h	dist	decay	dist	decay	dist	decay
1	$5.7012 \cdot 10^{-1}$	/	$5.4653 \cdot 10^{-1}$	/	$3.3175 \cdot 10^{-1}$	/
$\frac{1}{2}$	$5.9214 \cdot 10^{-2}$	3.2673	$5.7708 \cdot 10^{-2}$	3.2434	$3.2710 \cdot 10^{-2}$	3.3423
$\frac{1}{4}$	$6.1246 \cdot 10^{-3}$	3.2732	$6.1273 \cdot 10^{-3}$	3.2355	$3.4006 \cdot 10^{-3}$	3.2659
$\frac{1}{8}$	$6.9617 \cdot 10^{-4}$	3.1371	$6.9555 \cdot 10^{-4}$	3.1390	$3.8234 \cdot 10^{-4}$	3.1528
$\frac{1}{16}$	$8.3841 \cdot 10^{-5}$	3.0537	$8.2800 \cdot 10^{-5}$	3.0704	$4.5306 \cdot 10^{-5}$	3.0771
$\frac{1}{32}$	$1.0331 \cdot 10^{-5}$	3.0207	$1.0106 \cdot 10^{-5}$	3.0344	$5.5178 \cdot 10^{-6}$	3.0375

Table 3
The L^2 distances between $\mathbf{f}_h$, where $\mathbf{f}$ is defined in (26), and quintic ($m = 2$) alternative L^2 PH approximants (obtained by `Method` 1 and `Method` 2) and the nonlinear one, together with decay exponents (estimated approximation orders).

	`Method 1`		`Method 2`		`nonlinear`	
h	dist	decay	dist	decay	dist	decay
1	$1.3191 \cdot 10^{-1}$	/	$1.0940 \cdot 10^{-1}$	/	$5.1580 \cdot 10^{-2}$	/
$\frac{1}{2}$	$6.2373 \cdot 10^{-3}$	4.4025	$5.2976 \cdot 10^{-3}$	4.3681	$2.5569 \cdot 10^{-3}$	4.3343
$\frac{1}{4}$	$3.7251 \cdot 10^{-4}$	4.0656	$2.9265 \cdot 10^{-4}$	4.1781	$1.4153 \cdot 10^{-4}$	4.1752
$\frac{1}{8}$	$2.3420 \cdot 10^{-5}$	3.9915	$1.7289 \cdot 10^{-5}$	4.0813	$8.4634 \cdot 10^{-6}$	4.0637
$\frac{1}{16}$	$1.4668 \cdot 10^{-6}$	3.9969	$1.0521 \cdot 10^{-6}$	4.0384	$5.2059 \cdot 10^{-7}$	4.0230
$\frac{1}{32}$	$9.1630 \cdot 10^{-8}$	4.0008	$6.4919 \cdot 10^{-8}$	4.0186	$3.2313 \cdot 10^{-8}$	4.0100

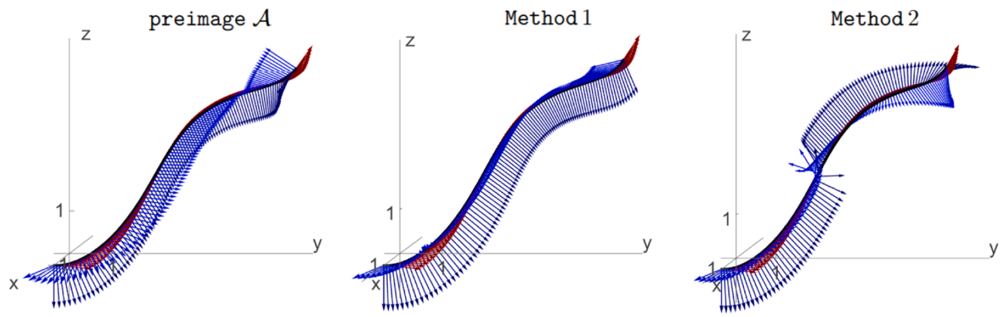

Fig. 4. PH curve $\mathbf{f}$ from Example 3 equipped with its ER frame (left) and orthonormal frames computed by `Method` 1 (middle) and `Method` 2 (right). The plots correspond to equidistant parameter values with step size $1/100$.

$$\mathcal{A}_3 = -\tfrac{3}{2} + 3\mathbf{i} + 2\mathbf{j} - \tfrac{1}{2}\mathbf{k}, \quad \mathcal{A}_4 = 1 + 3\mathbf{i} + \tfrac{1}{2}\mathbf{k}, \quad \mathbf{p}_0 = (1, 0, 0).$$

The curve is shown in Fig. 4 (left) together with its ER frame. The rotation–minimizing and the Frenet frames are also shown. The Frenet frame evidently exhibits substantial undesirable rotation about the tangent. Using the given preimage polynomial $\mathcal{A}$, the method reproduces the curve $\mathbf{f}$ exactly for degrees ≥ 9, as confirmed in Table 4. The table also lists the L^2 distances between $\mathbf{f}$ and its approximants computed by `Method` 1 and `Method` 2, and values of the functional E_ω. Note that the approximants obtained with `Method` 1 provide an efficient way to carry out degree reduction, while at the same time improving the properties of the associated ER frames.

6. Generalization to spatial Pythagorean–hodograph B–spline curves

As noted and examined in [2] for planar PH curves, employing piecewise polynomial functions for L^2 approximation provides an effective way to reduce the approximation error while maintaining a low polynomial degree and preserving the desired level of smoothness. In this section, we demonstrate that the ideas presented in [2] can also be extended to spatial curves. Namely, the construction from the previous section is generalized by replacing, in the preimage space, the subspace of real–valued polynomials $\mathbb{P}_m$ with a subspace of spline functions $\mathcal{S}_{m,\mathbf{t}}$ of degree m defined over the interval $[0, 1]$ partitioned by breakpoints $0 = \xi_0 < \xi_1 < \cdots <$

Table 4
L^2 distances between the PH curve $\mathbf{f}$ from Example 3 and its alternative L^2 PH approximants of different degrees, obtained by using the curve preimage polynomial, `Method 1` and `Method 2`. Values of E_ω are reported too.

	preimage $\mathcal{A}$		Method 1		Method 2	
m	dist	E_ω	dist	E_ω	dist	E_ω
1	$7.9084 \cdot 10^{-1}$	0.5990	$7.5036 \cdot 10^{-1}$	$5.2721 \cdot 10^{-2}$	$1.3165 \cdot 10^{0}$	18.236
2	$1.0780 \cdot 10^{-1}$	6.4790	$1.6115 \cdot 10^{-1}$	$4.5309 \cdot 10^{-1}$	$6.9286 \cdot 10^{-1}$	28.584
3	$4.9811 \cdot 10^{-2}$	6.2318	$5.4128 \cdot 10^{-2}$	$8.1543 \cdot 10^{-2}$	$4.8175 \cdot 10^{-1}$	33.930
4	0	8.2414	$1.0940 \cdot 10^{-2}$	$1.0738 \cdot 10^{-1}$	$3.0507 \cdot 10^{-1}$	51.629
5	0	8.2414	$4.1450 \cdot 10^{-3}$	$1.9572 \cdot 10^{-2}$	$2.8034 \cdot 10^{-1}$	46.708

$\xi_{N-1} < \xi_N = 1$ and equipped with the knot sequence $\mathbf{t}$, which determines the order of smoothness at the breakpoints:

$$\mathbf{t} = (t_\ell)_{\ell=0}^{d+m+1} = \left(0^{\langle m+1\rangle}, \xi_1^{\langle \nu_1\rangle}, \xi_2^{\langle \nu_2\rangle}, \ldots, \xi_{N-1}^{\langle \nu_{N-1}\rangle}, 1^{\langle m+1\rangle}\right), \quad d = m + \sum_{j=1}^{N-1} \nu_j. \tag{27}$$

Here $\xi_j^{\langle \nu_j\rangle}$ indicates that the breakpoint ξ_j is repeated ν_j-times. Specifically,

$$\mathcal{S}_{m,\mathbf{t}} = \operatorname{span}\left\{ B_{0,\mathbf{t}}^m, B_{1,\mathbf{t}}^m, \ldots, B_{d,\mathbf{t}}^m \right\},$$

where the B–spline basis functions $B_{k,\mathbf{t}}^m$ are defined recursively by

$$B_{j,\mathbf{t}}^m(t) = \omega_{j,m}(t)\, B_{j,\mathbf{t}}^{m-1}(t) + \left(1 - \omega_{j+1,m}(t)\right) B_{j+1,\mathbf{t}}^{m-1}(t), \qquad \omega_{j,m}(t) := \begin{cases} \frac{t-t_j}{t_{m+j}-t_j}, & t_j \neq t_{m+j}, \\ 0, & \text{otherwise}, \end{cases}$$

with

$$B_{j,\mathbf{t}}^0(t) = \begin{cases} 1, & t \in [t_j, t_{j+1}), \\ 0, & \text{otherwise}, \end{cases} \quad j = 0, 1, \ldots, d-1, \qquad B_{d,\mathbf{t}}^0(t) = \begin{cases} 1, & t \in [t_d, 1], \\ 0, & \text{otherwise}. \end{cases}$$

A spline function $p \in \mathcal{S}_{m,\mathbf{t}}$,

$$p(t) = \sum_{j=0}^{d} p_j\, B_{j,\mathbf{t}}^m(t),$$

with distinct inner knots, i.e., knots of multiplicity one, is of continuity class C^{m-1}. However, at the breakpoint ξ_j of multiplicity $\nu_j \geq 2$ the continuity is reduced to $C^{m-\nu_j}$. Choosing the initial and final knots of multiplicity $m+1$ ensures that $p(0) = p_0$ and $p(1) = p_d$. When $\nu_j = m - r$ for all $j = 1, 2 \ldots, N-1$ and a fixed $r \in \{0, 1 \ldots, m-1\}$, the spline is globally C^r continuous. In the case of equidistant breakpoints, we denote such a spline space by $\mathcal{S}_{m,N}^r$.

Spatial PH B–spline curves were introduced and studied in [6]. Following the approach therein, and adopting the notation employed in [2] for planar curves, the PH B–spline curves of degree n are constructed as follows. The preimage taken as $\mathcal{A} \in \mathcal{S}_{m,\mathbf{t}}(\mathbb{H})$, with $\mathbf{t}$ given by (27), defines the hodograph $\mathbf{h} = \mathcal{A}^{2\star}$, which lies in $\mathcal{S}_{2m,\tilde{\mathbf{u}}}(\mathbb{R}^3)$, where the knot sequence is

$$\tilde{\mathbf{u}} = (\tilde{u}_\ell)_{\ell=0}^{d_1+2m+1} = \left(0^{\langle 2m+1\rangle}, \xi_1^{\langle m+\nu_1\rangle}, \xi_2^{\langle m+\nu_2\rangle}, \ldots, \xi_{N-1}^{\langle m+\nu_{N-1}\rangle}, 1^{\langle 2m+1\rangle}\right), \quad d_1 = d + mN,$$

since the $\star$–operation doubles the degrees of the polynomial segments while preserving the order of continuity. Integrating the hodograph increases both the degree and the order of continuity by one, yielding the PH B–spline curve $\mathbf{p} \in \mathcal{S}_{n,\mathbf{u}}(\mathbb{R}^3)$, where

$$\mathbf{u} = (u_\ell)_{\ell=0}^{d_2+n+1} = (0, \tilde{\mathbf{u}}, 1), \quad n = 2m+1, \quad d_2 = d_1 + 1,$$

and

$$\mathbf{p}(t) = \int_0^t \mathbf{h}(\tau)\, d\tau + \mathbf{p}_0 = \sum_{j=0}^{d_2} \mathbf{p}_j\, B_{j,\mathbf{u}}^n(t).$$

As in Section 5, to construct the alternative L^2 approximant for a given spatial curve $\mathbf{f}$, one first needs to determine its preimage curve $\mathcal{A}_\mathbf{f} : [0,1] \to \mathbb{H}$ as previously described. To compute for $\mathcal{A}_\mathbf{f}$ its L^2 approximant $\mathcal{A} \in \mathcal{S}_{m,\mathbf{t}}(\mathbb{H})$, represented as $\mathcal{A}(t) = \sum_{j=0}^d \mathcal{A}_j B_{j,\mathbf{t}}^m(t)$, one solves the linear system of equations

$$\mathbf{G}\,(\mathcal{A}_j)_{j=0}^d = \mathbf{g}, \quad \mathbf{G} = \left(\left\langle B_{k,\mathbf{t}}^m, B_{j,\mathbf{t}}^m \right\rangle\right)_{j,k=0}^d, \quad \mathbf{g} = \left(\left\langle \mathcal{A}_\mathbf{f}, B_{j,\mathbf{t}}^m \right\rangle\right)_{j=0}^d,$$

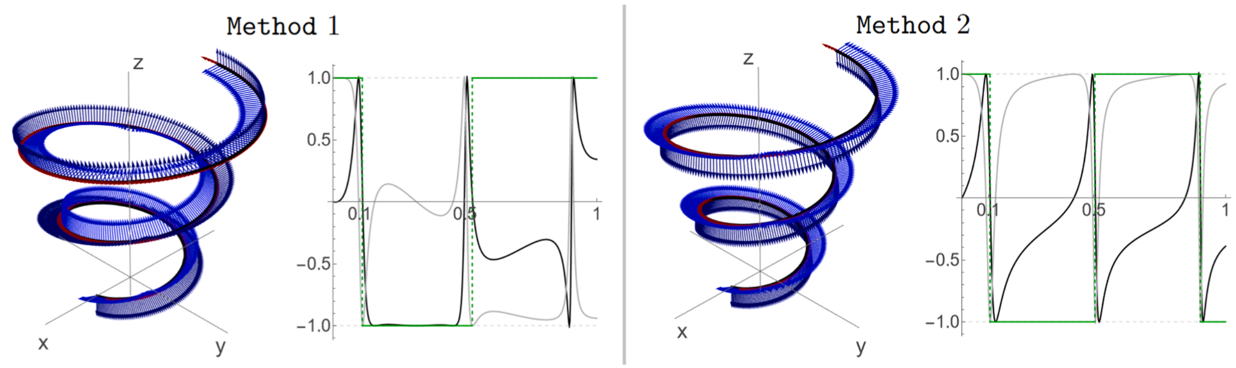

Fig. 5. Exponential spiral from Example 4 equipped with orthonormal frames computed by Method 1 (left) and Method 2 (right), together with graphs of functions v_2 (black) and v_3 (gray) that determine $\mathcal{W}$ by (4), and the sign function ς (green), used in (24a).

Table 5
L^2 errors of the alternative L^2–PH B–spline approximants computed based on Method 1 and Method 2 for different number N of polynomial segments and different types of spline spaces.

	cubic C^1 splines		quintic C^2 splines		quintic C^1 splines	
N	Method 1	Method 2	Method 1	Method 2	Method 1	Method 2
5	$4.659 \cdot 10^{-1}$	$4.386 \cdot 10^{-1}$	$1.603 \cdot 10^{-1}$	$1.352 \cdot 10^{-1}$	$2.619 \cdot 10^{-2}$	$2.528 \cdot 10^{-2}$
10	$2.399 \cdot 10^{-2}$	$2.318 \cdot 10^{-2}$	$3.507 \cdot 10^{-3}$	$3.267 \cdot 10^{-3}$	$1.779 \cdot 10^{-3}$	$1.702 \cdot 10^{-3}$
15	$5.095 \cdot 10^{-3}$	$4.969 \cdot 10^{-3}$	$4.849 \cdot 10^{-4}$	$4.580 \cdot 10^{-4}$	$3.220 \cdot 10^{-4}$	$3.080 \cdot 10^{-4}$
20	$1.791 \cdot 10^{-3}$	$1.761 \cdot 10^{-3}$	$1.257 \cdot 10^{-4}$	$1.194 \cdot 10^{-4}$	$9.313 \cdot 10^{-5}$	$8.882 \cdot 10^{-5}$
25	$8.092 \cdot 10^{-4}$	$7.970 \cdot 10^{-4}$	$4.492 \cdot 10^{-5}$	$4.282 \cdot 10^{-5}$	$3.544 \cdot 10^{-5}$	$3.384 \cdot 10^{-5}$
30	$4.246 \cdot 10^{-4}$	$4.184 \cdot 10^{-4}$	$1.953 \cdot 10^{-5}$	$1.865 \cdot 10^{-5}$	$1.597 \cdot 10^{-5}$	$1.527 \cdot 10^{-5}$
35	$2.466 \cdot 10^{-4}$	$2.431 \cdot 10^{-4}$	$9.698 \cdot 10^{-6}$	$9.273 \cdot 10^{-6}$	$8.109 \cdot 10^{-6}$	$7.756 \cdot 10^{-6}$
40	$1.541 \cdot 10^{-4}$	$1.520 \cdot 10^{-4}$	$5.298 \cdot 10^{-6}$	$5.070 \cdot 10^{-6}$	$4.498 \cdot 10^{-6}$	$4.304 \cdot 10^{-6}$

where $\mathbf{G}$ is a banded Gram matrix. The PH B–spline approximant $\mathbf{p} \in \mathcal{S}_{n,\mathbf{u}}(\mathbb{R}^3)$ is then obtained from $\mathcal{A}$ using the $\star$-operation and the integration as explained above. The boundary point $\mathbf{p}_0$ is determined as in the polynomial case by the minimization

$$\mathbf{p}_0^* = \underset{\mathbf{p}_0 \in \mathbb{R}^3}{\operatorname{argmin}} \|\mathbf{f} - \mathbf{p}\|,$$

which yields (see [2, Section 5] for the proof)

$$\mathbf{p}_0^* = \sum_{j=0}^{d_2} \left(\int_0^1 \mathbf{f}(t) B_{j,\mathbf{u}}^n(t)\, dt \right) - \sum_{j=1}^{d_2} \left(\sum_{\ell=0}^{j-1} \frac{\widetilde{u}_{\ell+n} - \widetilde{u}_\ell}{n} \mathbf{h}_\ell \right) \left(\sum_{k=0}^{d_2} \int_0^1 B_{k,\mathbf{u}}^n(t) B_{j,\mathbf{u}}^n(t)\, dt \right).$$

Here $\mathbf{h}_\ell$ are the B-coefficients of the hodograph. For more details on their computation from the preimage B-coefficients $\mathcal{A}_\ell$, the reader is referred to [2,6].

The following examples demonstrate the theoretical results and illustrate the effectiveness of the proposed method. For the preimage spline spaces we select $S^0_{1,N}(\mathbb{H})$, $S^1_{2,N}(\mathbb{H})$ and $S^0_{2,N}(\mathbb{H})$, yielding PH spline curves from $S^1_{3,N}(\mathbb{R}^3)$, $S^2_{5,N}(\mathbb{R}^3)$ and $S^1_{5,N}(\mathbb{R}^3)$, respectively — that is cubic C^1, quintic C^2, and quintic C^1 PH spline curves.

Example 4. Let the curve $\mathbf{f}$ be chosen as an exponential spiral

$$\mathbf{f}(t) = \left(2e^t \cos(5\pi t), 2e^t \sin(5\pi t), 10t\right), \quad t \in [0,1]. \tag{28}$$

To equip it with an orthonormal frame we apply Method 1 (rotation minimizing frame) and Method 2 (Frenet frame). The frames are shown in Fig. 5, together with graphs of the functions v_2 and v_3 needed to determine the preimage $\mathcal{A}_\mathbf{f}$. Note that the value of E_ω for the Frenet frame is 10.2655. The alternative cubic C^1, quintic C^2, and quintic C^1 L^2–PH B–spline approximants with $N = 5$ polynomial segments are shown in Fig. 6, where the preimage curve $\mathcal{A}_\mathbf{f}$ is computed based on the rotation minimizing frame. Corresponding graphs of approximants computed using the Frenet frame are omitted, since only small visible differences can be observed. This is also confirmed by Table 5 that provides the L^2 errors for different numbers N of polynomial segments. Fig. 7 (left) shows the L^2 errors on a logarithmic scale for all three spline spaces in dependence of the dimension of the preimage spline space (denoted by NDOF), which equals $N+1$, $N+2$ and $2N+1$, respectively. Values of E_ω tend to zero for approximants computed using Method 1, and to the value 10.2655 for approximants computed using Method 2, as illustrated in Fig. 7.

Example 5. As a final example, we use $N+1 = 16$ equidistant breakpoints on $[0,1]$ and choose $\mathbf{f}$ as a C^2 cubic spline with control points

$$(0.01, -1, 0.23),\ (0.41, -0.88, 1.5),\ (0.72, -0.77, 2.77),\ (0.78, -0.65, 4.38),\ (0.57, -0.55, 4.91),$$

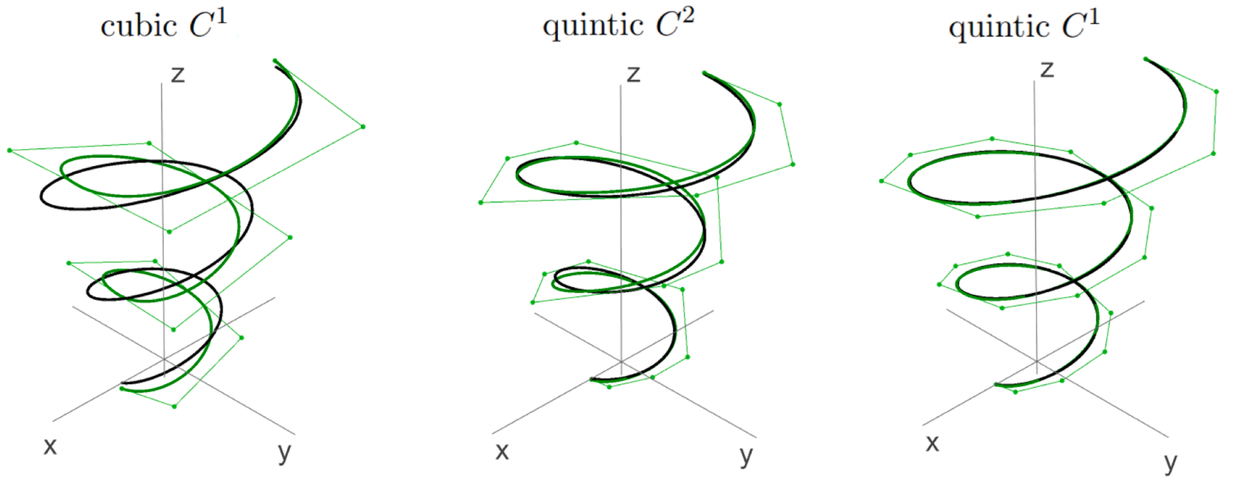

Fig. 6. L^2–PH B–spline approximants for the curve (28), belonging to $\mathcal{S}_3^1(\mathbb{R}^3)$, $\mathcal{S}_5^2(\mathbb{R}^3)$ and $\mathcal{S}_5^1(\mathbb{R}^3)$, computed using the preimage $\mathcal{A}_{\mathbf{f}}$ obtained by `Method 1` (rotational minimizing frame), using $N = 5$ polynomial segments.

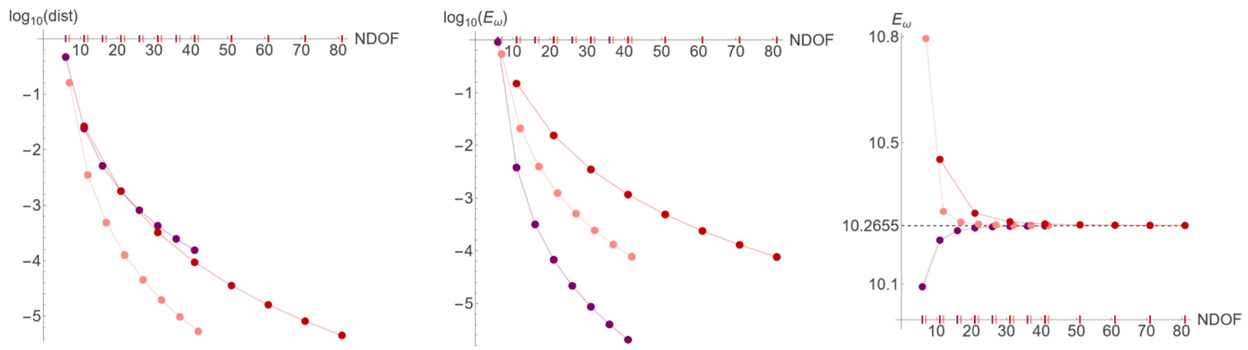

Fig. 7. Left: L^2 errors in a logarithmic scale for cubic C^1 (purple color), quintic C^2 (pink color) and quintic C^1 (red color) alternative L^2–PH B–spline approximants computed based on `Method 1` in dependence of the NDOF of the preimage spline space. Middle: Values of E_ω in a logarithmic scale for approximants computed using `Method 1`. Right: Values of E_ω for approximants computed using `Method 2`.

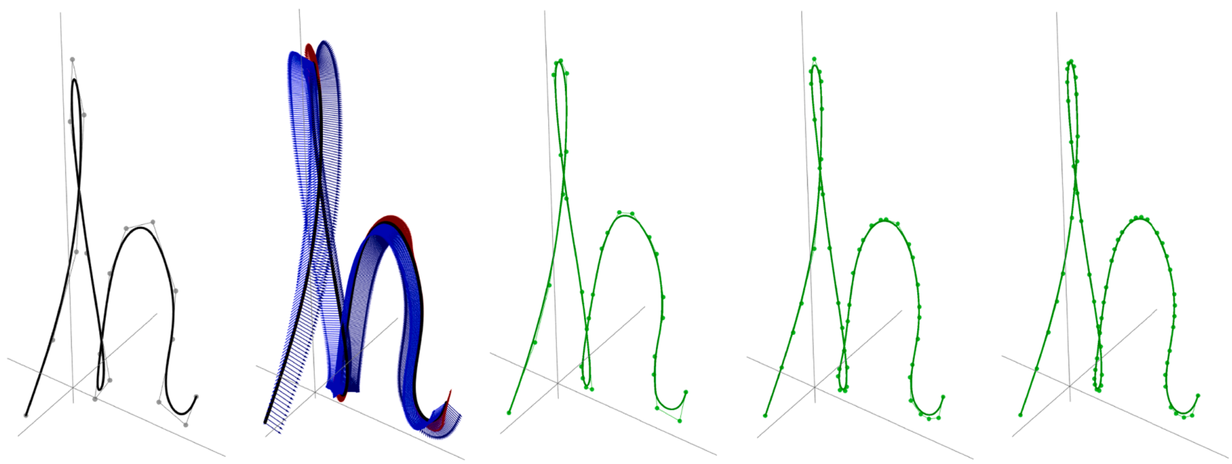

Fig. 8. Cubic C^2 spline from Example 5 (left), its rotation–minimizing frame, and alternative L^2–PH B–spline approximants belonging to $\mathcal{S}_{3,N}^1(\mathbb{R}^3)$, $\mathcal{S}_{5,N}^2(\mathbb{R}^3)$ and $\mathcal{S}_{5,N}^1(\mathbb{R}^3)$. For all splines, the gray and green points represent the control points (B–coefficients).

$$(0.44, -0.45, 4.16),\ (0.55, -0.35, 2.49),\ (0.81, -0.27, 0.67),\ (0.51, -0.19, 0.17),\ (0.56, -0.13, 0.89),$$
$$(0.69, -0.08, 2.12),\ (0.9, -0.04, 2.79),\ (1.25, -0.01, 2.97),\ (1.58, 0, 2.15),\ (1.56, 0, 1.45),$$
$$(1.4, -0.02, 0.42),\ (1.82, -0.05, 0.27),\ (1.97, -0.09, 0.82).$$

We approximate it with L^2–PH B–splines from $\mathcal{S}^1_{3,N}(\mathbb{R}^3)$, $\mathcal{S}^2_{5,N}(\mathbb{R}^3)$ and $\mathcal{S}^1_{5,N}(\mathbb{R}^3)$, computed using the rotation–minimizing frame, shown in Fig. 8, together with $\mathbf{f}$ (left) and the computed approximants. The corresponding L^2 distances are 9.5432×10^{-3}, 7.1342×10^{-3}, and 1.3608×10^{-3}, respectively. These approximation errors clearly reflect the number of degrees of freedom involved (the dimensions of the preimage spaces are $\dim \mathcal{S}^0_{1,N} = 16$, $\dim \mathcal{S}^1_{2,N} = 17$ and $\dim \mathcal{S}^0_{2,N} = 31$). Note also that the ER frames of the approximating PH B–splines remain close to rotation–minimizing ones, as indicated by the corresponding values 0.44032, 0.10733, and 0.023744 of the functional E_ω, respectively.

7. Closure

Algorithms for approximating a given space curve by a spatial PH curve have been proposed and demonstrated by representative computed examples. Direct L^2 approximation in $\mathbb{R}^3$ involves the solution of non–linear systems of equations, which are computation–intensive and potentially dependent on appropriate initial estimates for the solution values. An alternative approach, based on L^2 approximation in the quaternion preimage space of spatial PH curves, incurs only linear systems of equations that admit efficient and reliable solution schemes. Since the preimage of a given curve in $\mathbb{R}^3$ under the PH map is a surface in $\mathbb{R}^4$, an appropriate locus on that surface must be selected for comparison with the PH curve quaternion preimage polynomial. The selection is motivated by the observation that PH curves which admit rational rotation–minimizing frames correspond to preimages that are geodesics on the surface. To utilize this observation, a simple established method for approximating the RMF on any given smooth curve is employed, which can achieve any desired accuracy by increasing the sampling density.

Possible directions for further research include imposing additional interpolation constraints and investigating the influence of the parameterization of the given curve on the approximation accuracy. Another promising topic is the generalization of polynomial PH curves to rational PH curves or to PH curves based on mixed polynomial-trigonometric bases. Moreover, considering L^2 approximation for discrete data sets, rather than continuous curves, may also be of interest.

Declaration of competing interest

The authors declare that they have no known competing financial interests or personal relationships that could have appeared to influence the work reported in this paper.

Acknowledgements

Research on this paper has been partly supported by the research programs P1–0288 and P1–0404, and the research grants N1–0237 and N1–0296, of the Slovenian Research and Innovation Agency.

Data availability

All data used in this study are provided in the manuscript.

References

[1] R.T. Farouki, Pythagorean–Hodograph Curves: Algebra and Geometry Inseparable, Springer, Berlin, 2008.
[2] R.T. Farouki, M. Knez, V. Vitrih, E. Žagar, On L^2 approximation by planar Pythagorean–hodograph curves, Math. Comput. Simul. 233 (2025) 296–310.
[3] W. Wang, B. Jüttler, D. Zheng, Y. Liu, Computation of rotation–minimizing frames, ACM Trans. Graph. 27 (2008) article 2.
[4] R.T. Farouki, T. Sakkalis, Pythagorean–hodograph space curves, Adv. Comput. Math. 2 (1994) 41–66.
[5] H.I. Choi, D.S. Lee, H.P. Moon, Clifford algebra, spin representation, and rational parameterization of curves and surfaces, Adv. Comput. Math. 17 (2002) 5–48.
[6] G. Albrecht, C.V. Beccari, L. Romani, Spatial Pythagorean–hodograph B–spline curves and 3D point data interpolation, Comput. Aided Geom. Des. 80 (2020) 101868.
[7] R.T. Farouki, Existence of Pythagorean–hodograph quintic interpolants to spatial G^1 Hermite data with prescribed arc lengths, J. Symb. Comput. 95 (2019) 202–216.
[8] R.T. Farouki, M. al Kandari, T. Sakkalis, Hermite interpolation by rotation–invariant spatial Pythagorean–hodograph curves, Adv. Comput. Math. 17 (2002) 369–383.
[9] R.T. Farouki, C. Giannelli, C. Manni, A. Sestini, Identification of spatial PH quintic Hermite interpolants with near–optimal shape measures, Comput. Aided Geom. Des. 25 (2008) 274–297.
[10] R.T. Farouki, M. Knez, V. Vitrih, E. Žagar, Spatial C^2 closed loops of prescribed arc length defined by spatial Pythagorean–hodograph curves, Appl. Math. Comput. 391 (2021) 125653.
[11] R.T. Farouki, C. Manni, M.L. Sampoli, A. Sestini, Shape-preserving interpolation of spatial data by Pythagorean–hodograph quintic spline curves, IMA J. Numer. Anal. 35 (2015) 478–498.
[12] C. Giannelli, L. Sacco, A. Sestini, Interpolation of 3D data streams with C^2 PH quintic splines, Adv. Comput. Math. 48 (2022) 61.
[13] M. Huard, R.T. Farouki, N. Sprynski, L. Biard, C^2 interpolation of spatial data subject to arc–length constraints using Pythagorean–hodograph quintic splines, Graph. Models 76 (2014) 30–42.
[14] M. Knez, G^1 motion interpolation using cubic PH biarcs with prescribed length, Comput. Aided Geom. Des. 67 (2018) 21–33.
[15] M. Knez, F. Pelosi, M.L. Sampoli, Construction of G^2 spatial interpolants with prescribed arc lengths, J. Comput. Appl. Math. 441 (2024) 115684.
[16] Z. Šír, B. Jüttler, C^2 Hermite interpolation by Pythagorean hodograph curves, Math. Comput. 76 (2007) 1373–1391.

[17] H.I. Choi, C.Y. Han, Euler–Rodrigues frame on spatial Pythagorean–hodograph curves, Comput. Aided Geom. Des. 19 (2002) 603–620.
[18] B. Jüttler, M.G. Wagner, Kinematics and animation, in: G. Farin, J. Hoschek, M.-S. Kim (Eds.), Handbook of Computer Aided Geometric Design, Elsevier, Amsterdam, 2002, pp. 723–748.
[19] B. Bastl, B. Jüttler, M. Lávička, T. Schultz, Z. Šír, On the parameterization of rational ringed surfaces and rational canal surfaces, Math. Comput. Sci. 8 (2014) 299–319.
[20] R.T. Farouki, R. Gutierrez, Geometry of the ringed surfaces in $\mathbb{R}^4$ that generate spatial Pythagorean hodographs, J. Symb. Comput. 73 (2016) 87–103.
[21] R.T. Farouki, M. al Kandari, T. Sakkalis, Structural invariance of spatial Pythagorean hodographs, Comput. Aided Geom. Des. 19 (2002) 395–407.
[22] R.T. Farouki, Quaternion and Hopf map characterizations for the existence of rational rotation–minimizing frames on quintic space curves, Adv. Comput. Math. 33 (2010) 331–348.
[23] R.T. Farouki, G. Gentili, C. Giannelli, A. Sestini, C. Stoppato, A comprehensive characterization of the set of polynomial curves with rational rotation–minimizing frames, Adv. Comput. Math. 43 (2017) 1–24.
[24] H. Guggenheimer, Computing frames along a trajectory, Comput. Aided Geom. Des. 6 (1989) 77–78.
[25] R.T. Farouki, Exact rotation–minimizing frames for spatial Pythagorean–hodograph curves, Graph. Models 64 (2003) 382–395.
[26] R.T. Farouki, C. Giannelli, A. Sestini, Identification and "reverse engineering" of Pythagorean–hodograph curves, Comput. Aided Geom. Des. 34 (2015) 21–36.
[27] Z. Li, J. Schicho, H.-P. Schröcker, The rational motion of minimal dual quaternion degree with prescribed trajectory, Comput. Aided Geom. Des. 41 (2016) 1–9.
[28] H.-P. Schröcker, Z. Šír, Three paths to rational curves with rational arc length, Appl. Math. Comput. 478 (2024) 128842.